NASA-CR-196103

ALLEVIATION OF WHIRL-FLUTTER ON A JOINED-WING TILT-ROTOR AIRCRAFT CONFIGURATION USING ACTIVE CONTROLS

N94-36436
Unclas
G3/08 0013777
(NASA-CR-196103) ALLEVIATION OF WHIRL-FLUTTER ON A JOINED-WING TILT-ROTOR AIRCRAFT CONFIGURATION USING ACTIVE CONTROLS (Sterling Software) 27 p

Johannes M van Aken
Aerospace Engineer

Sterling Software
Rotorcraft Aeromechanics Branch
NASA Ames Research Center

JUN 28 1994
NCC 2-417
FINAL

Presented at the International Specialists' Meeting on Rotorcraft Basic Research of the American Helicopter Society, Atlanta, Georgia, March 25-27, 1991

TO: CASI

ALLEVIATION OF WHIRL-FLUTTER ON A JOINED-WING TILT-ROTOR AIRCRAFT CONFIGURATION USING ACTIVE CONTROLS

Johannes M. van Aken

Aerospace Engineer
Sterling Software
Rotorcraft Aeromechanics Branch
NASA Ames Research Center

ABSTRACT

The feasibility of using active controls to delay the onset of whirl-flutter on a joined-wing tilt-rotor aircraft was investigated. The CAMRAD/JA code was used to obtain a set of linear differential equations, which describe the motion of the joined-wing tilt-rotor aircraft. The hub motions due to wing/body motion is a standard input to CAMRAD/JA and were obtained from a structural dynamics model of a representative joined-wing tilt-rotor aircraft. The CAMRAD/JA output, consisting of the open-loop system matrices, and the airframe free-vibration motion were input to a separate program, which performed the closed-loop, active control calculations. An eigenvalue analysis was performed to determine the flutter stability of both open- and closed-loop systems. Sensor models, based upon the feedback of pure state variables and based upon hub-mounted sensors, providing physically measurable accelerations, were evaluated. It was shown that the onset of tilt-rotor whirl-flutter could be delayed from 240 to above 270 knots by feeding back vertical and span-wise accelerations, measured at the rotor hub, to the longitudinal cyclic pitch. Time response calculations at a 270-knot cruise condition showed an active cyclic pitch control level of 0.009 deg, which equates to a very acceptable 9-pound active-control force applied at the rotor hub.

NOMENCLATURE

A_i (i=0,1,2)	system matrix
A	first-order system matrix
B_0	control matrix
B	first-order control matrix
C_i (i=0,1,2)	system sensor matrix
D_0	control sensor matrix
F	feedback gain matrix
g_m	noise level gain vector
M	modal matrix
q_k	k^{th} generalized coordinate
$r_{cg,p}$	position vector of point P in a CAMRAD/JA body axis system with origin at the aircraft center of gravity, ft
u_p	airframe linear displacement at location P
v	control vector
V_{trim}	aircraft trim velocity vector
w	sensor noise vector
x	state vector
x_s	first-order state variable
y	sensor vector
δ_s	longitudinal cyclic pitch, deg
λ	eigenvalue
Λ	diagonal eigenvalue matrix
θ	pitch angle, deg
θ_p	airframe angular displacement at location P
ϕ	roll angle, deg
ψ	yaw angle, deg
ζ	damping ratio
ξ_k	k^{th} linear displacement vector
γ_k	k^{th} angular displacement vector
ω	angular velocity perturbation vector
ω_n	natural frequency
Ω	rotor rotation rate, rad/sec

Indices:

a	anti-symmetric mode
ac	active control
cg	center of gravity
F	airframe body axis system
FT	trim Euler angles
p	pilot control, or airframe location P
h	hub
h,c	hub motion , chord-wise direction
h,s	hub motion , span-wise direction
h,v	hub motion, vertical direction
s	symmetric mode

Presented at the International Specialists' Meeting on Rotorcraft Basic Research of the American Helicopter Society, Atlanta, Georgia, March 25-27, 1991.
This work is declared a work of the U.S. Government and is in the public domain.

PRECEDING PAGE BLANK NOT FILMED

INTRODUCTION

The goal of the tilt-rotor concept is to achieve the cruise speed of a fixed-wing aircraft, while retaining the hover capability of a helicopter. Current tilt-rotor aircraft (XV-15 and V-22) employ very thick wing airfoils (23% thick) to obtain adequate wing stiffness and strength to handle the loads imposed by vertical-jump takeoffs and high speed whirl-flutter stability. These thick airfoils result in wing compressibility effects limiting the high speed potential of the tilt-rotor aircraft, e.g. to M=0.575 for a XV-15 size aircraft. In hover flight the net thrust of the tilt-rotor aircraft is reduced by the vertical drag (download) of the wing[1]. Wolkovitch, et. al.[2], performed an analytical study to evaluate the application of the joined-wing concept[3] to tilt-rotor aircraft. Figure 1 shows the baseline cantilever-wing tilt-rotor configuration, representing a XV-15 size tilt-rotor aircraft. Figure 2 shows a typical joined-wing tilt-rotor configuration studied in Ref. 2. The joined wing concept can reduce the projected wing area in the rotor downwash in hover, thus potentially reducing the hover download. The joined wing concept also allows for thinner airfoil sections (12% thick), resulting in an increase in the drag-divergence limiting Mach number from 0.575 for the cantilever-baseline model to 0.69 for the joined-wing model.

Reference 2 evaluated various joined-wing tilt-rotor configurations in terms of potential performance improvements, airframe aeroelastic characteristics, and aircraft whirl flutter speeds. Design parameters that were varied included front wing sweep angle, front wing airfoil thickness, and nacelle center of gravity location.

Reference 2 showed a potential speed increase of 100 knots by delaying the compressibility drag effects to higher Mach numbers. However, this performance advantage was negated by a lowering of the joined-wing whirl-flutter speed from 330 to 240 knots. Representative results for Ref. 2 are shown in Fig. 3.

Studies have been performed in the use of active controls to reduce a tilt-rotor's response to a gust[4-7] and to reduce tilt-rotor blade loads during maneuvers[8]. Other studies have been performed to improve the hover aeromechanical stability of helicopters[9]. Clearly an area of interest for tilt-rotors is flutter control with the objective to allow the tilt-rotor aircraft to fly at higher speeds or to reduce its structural weight.

Nasu[10] studied flutter control on a simplified tilt-rotor model, consisting of a semi-span straight wing, a pylon attached to the wing tip, and a three-bladed hingeless rotor. Nasu considered symmetric wing elastic motion (wing beamwise, chordwise, and torsional bending) and rotor blade chordwise and flapwise bending. His feedback control was performed in the state-space domain. The author studied the use of active controls to delay the aeroelastic instability (whirl-flutter) on a tilt-rotor model, representative of a XV-15 size aircraft[11].

The results of a whirl-flutter alleviation study for a joined-wing tilt-rotor aircraft are presented here. Table 1 provides a comparison of the tilt-rotor models studied in Refs. 10 and 11 with the present investigation. This study included rigid-body motion, both symmetric and anti-symmetric elastic body degrees of freedom, rotor blade bending and torsion modes, the hub gimbal and the rotor speed degrees of freedom. In addition, feedback control in the state-space domain as well as feedback control using realistic sensor models (the output of hub-mounted accelerometers) was investigated.

INVESTIGATION APPROACH

The approach followed in this joined-wing tilt-rotor whirl flutter alleviation study is described in this section and is schematically shown in Fig. 4.

A number of XV-15 size joined-wing tilt-rotor configurations were studied in Ref. 2, which used the structural analysis code MSC-PAL to calculate the airframe mode shapes, modal frequency, and modal mass. Only the airframe mode shape at the hub is reported in Ref. 2.

A typical joined-wing tilt-rotor aircraft configuration (model 166CL in Ref. 2) was selected to study the potential of using active controls to delay the occurrence of whirl flutter on a joined-wing tilt-rotor. The airframe structural dynamic characteristics, consisting of the modal frequency, modal mass, and the hub motion due to elastic airframe deformation were obtained from Ref. 2 and are used as an input to the rotorcraft analysis code CAMRAD/JA, which provided the mathematical plant model of the tilt-rotor aircraft. The CAMRAD/JA analysis was also used in Ref. 2 to determine the whirl flutter speed for the various joined-wing tilt-rotor aircraft configurations. The CAMRAD/JA (Comprehensive Analytical

Model of Rotorcraft Aerodynamics and Dynamics, Johnson Aeronautics) is described in detail in Refs. 12-15 and a summary description is provided in Appendix A.

CAMRAD/JA is used to develop the equations of motion for the airframe motion, the equations of motion for the rotor, and the expressions for the rotor hub load reactions. The coupled airframe-rotor equations of motion are obtained by substituting the hub motion into the equations for the rotor motion and hub loads, and then substituting the hub reactions into the airframe equations of motion. The aircraft motion consists of the six rigid body degrees of freedom and the airframe elastic free-vibration modes. CAMRAD/JA accounts for the rigid body motion in a quasi-static manner. The CAMRAD/JA analysis specifically uses the MSC-PAL data in modeling the airframe dynamics at the rotor hub location due to the elastic airframe deformation.

For purposes of an aeroelastic analysis, CAMRAD/JA linearizes the aerodynamic and inertial forces around the aircraft trim solution to derive a mathematical plant model, consisting of a set of linear differential equations describing the perturbed motion of the aircraft about the trim condition.

The CAMRAD/JA plant model was used as an input to a separate program, which allowed for the evaluation of various feedback control system schemes for their effectiveness in delaying the occurrence of whirl-flutter. Additional input to the closed-loop analysis program consisted of the motion sensor model and the active control feedback specifications. The analysis code uses an eigenvalue analysis to determine the stability of the closed-loop system and allows for the calculation of the system time-history response to various types of control inputs, such as an impulse or step control input.

A separate utility was used to obtain a mathematical formulation describing the output of the airframe-mounted motion sensors. Input to this utility consisted of the geometric definition of the sensor location on the airframe, the airframe mode shape data for the sensor location, and CAMRAD/JA parameters describing the aircraft trim conditions (i.e., the aircraft velocity and orientation, and its flight path).

Sensor models, based on pure state variable domain feedback as well as based on realistic sensors, measuring the actual "physical" motion of the airframe at the hub were evaluated. An eigenvalue analysis was used to determine the stability of the aircraft with the closed-loop feedback system. Time response calculations were performed to determine the magnitude/level of the required active control inputs. The effect of sensor noise on the closed-loop aircraft stability was also investigated using random noise of a specified magnitude to simulate measurement noise and/or system modelling uncertainty.

THEORETICAL FORMULATION

PLANT MODEL DEVELOPMENT

For the purpose of performing an aeroelastic stability analysis, the rotorcraft motion can be described by means of a set of linear differential equations of the form[12]:

$$A_2\ddot{x} + A_1\dot{x} + A_0x = B_0v \qquad (1)$$

where x is the vector of degrees of freedom, v is the vector of controls, A_i (i=0,1,2) are the system matrices, and B_0 is the control matrix. Equation (1) represents the rotorcraft plant model, i.e., the tilt-rotor aircraft without feedback control, referred to hereafter as the basic aircraft. The A_i (i=0,1,2) and B_0 matrices are obtained from the CAMRAD/JA code and are a function of the cruise flight conditions. For the most general case in which Eqn. (1) describes the motion of a rotorcraft, the matrices A_i (i=0,1,2) and B_0 have periodic coefficients and must be analyzed for stability by the methods of Floquet-Liapunov theory. For the tilt-rotor in cruise flight, the rotor operates in a mostly axial-flow environment and the A_i (i=0,1,2) and B_0 matrices in Eqn. (1) are constant coefficient matrices. Consequently, the techniques for the analysis of time-invariant systems can be used[16].

The CAMRAD/JA basic aircraft plant model matrices (Eqn. (1)) are input to the closed-loop analysis code which models the airframe motion sensor outputs and feedback control system as described by Eqns. (2)-(8) below.

The control vector v in Eqn. (1) consists of the sum of the pilot control inputs, v_p, and the active control inputs, v_{ac}:

$$v(t) = v_p(t) + v_{ac}(t) \qquad (2)$$

The motion sensor output is described by the observer or sensor vector, y, which is defined as:

$$y = C_2\ddot{x} + C_1\dot{x} + C_0x + D_0v \qquad (3)$$

where C_i (i=0,1,2) are the system sensor matrices and D_0 is the control sensor matrix.

The active control vector, v_{ac}, is defined by:

$$v_{ac} = Fy \qquad (4)$$

where F is the output feedback gain matrix. No attempt is made here to model the dynamics of the swashplate actuators.

Combining Eqns. (3) and (4) and substituting (v_p+v_{ac}) for v in Eqn. (1) leads to the following equation for the closed-loop system:

$$(A_2-B_0FC_2)\ddot{x} + (A_1-B_0FC_1)\dot{x} + (A_0-B_0FC_0)x = (B_0+B_0FD_0)v \qquad (5)$$

which can be rewritten as:

$$A_2^*\ddot{x} + A_1^*\dot{x} + A_0^*x = B_0^*v \qquad (6)$$

Equation (6) is transformed to a first-order state variable form by the substitution:

$$x_s = \begin{pmatrix} \dot{x} \\ x \end{pmatrix} \qquad (7)$$

yielding:

$$\dot{x}_s = Ax_s + Bv \qquad (8)$$

An eigenvalue analysis can be performed to determine the stability of the rotorcraft system represented in the state-space form by Eqn. (8). The natural frequency, ω_n, and the damping ratio, ζ (fraction of critical damping), for each mode is obtained from the associated eigenvalue, λ, as $\omega_n=|\lambda|\Omega/2\pi$ and $\zeta=-Real(\lambda)/|\lambda|$, respectively, where Ω is the rotor rpm in rad/sec.

SENSOR MODEL

The sensor model used in the feedback control system is defined by Eqn. (3). By appropriate selection of the elements of the C_i (i=0,1,2) by setting the elements to "1" or "0", a feedback scheme based upon pure state variables can be obtained. Alternatively, the output of a sensor, such as an accelerometer mounted on the airframe can be modeled by the proper specification of the elements of the C_i matrices. The coefficients in the j^{th} row of the C_i matrices represent the contribution of each aircraft degree of freedom to the sensor output signal represented by the corresponding j^{th} element of the sensor vector y.

The contribution of k^{th} aircraft degree of freedom to the output of a sensor located at a point P can be the due to the local airframe displacement, $x_{p,k}$, (through the corresponding C_0-matrix element), the velocity at point P, $\dot{x}_{p,k}$ (C_1-matrix element), or its acceleration $\ddot{x}_{p,k}$ (C_2-matrix element).

It is assumed that single-direction motion sensors are employed in the sensor model. Therefore each element of the sensor vector y represents the motion of point P in only one direction. Only airframe-mounted sensors are considered. The rotor degrees of freedom do not contribute to the sensor output.

To determine the element values of the C_i-matrices (i=0,1,2) it is necessary to determine the aircraft body motion at point P where the sensor is located. The derivation for this body motion at point P follows the derivation for the hub motion as presented in Ref. 12 and is described below.

The body axis system is defined as pictured in Fig. 5. From the pilot's perspective the body x-axis is defined positive forward, the body y-axis is positive to the right, and the body z-axis is positive downward. Assume that the sensor is located at a point P, whose location with respect to the reference body axis system is given by the position vector r_p. The sensor at point P will sense the motion (displacement, velocity and/or acceleration) at P due to both the rigid aircraft and airframe elastic motions. The motion at point P on the aircraft in flight is given by the linear displacement vector, u_p, and the angular displacement vector, θ_p. These displacements at point P are obtained by expanding the motion at point P in a series of orthogonal free vibration modes, in which the first six modes represent the rigid body motion:

$$u_p(r_p,t) = \sum_{k=1}^{\infty} q_k(t)\xi_k(r_p) \qquad (9)$$

$$\theta_p(r_p,t) = \sum_{k=1}^{\infty} q_k(t)\gamma_k(r_p) \qquad (10)$$

The orthogonality property of the modes implies that the elastic airframe modes produce no net displacement of the aircraft center of gravity.

The first six degrees of freedom in Eqns. (9) and (10) represent the rigid body motions. The generalized coordinates q_1, q_2, and q_3 are the rigid body angular motion around the x-axis (roll ϕ, positive right side down), around the y-axis (pitch θ, positive nose up), and around the z-axis (yaw ψ, positive nose to the right), respectively. The generalized coordinates q_4, q_5, and q_6 are the body linear motions along the x-, y-, and z-axis, respectively. The rigid body motion can be specified by the linear perturbation velocity of the body center of gravity and the angular perturbation velocity of the body around the body c.g. The linear velocity perturbation of the body center of gravity is given by:

$$\dot{u}_{cg,rigid} = \begin{pmatrix} \dot{x}_F \\ \dot{y}_F \\ \dot{z}_F \end{pmatrix} \tag{11}$$

and the rigid body angular velocity perturbation is given by:

$$\omega_F = [R_{FT}] \begin{pmatrix} \dot{\phi}_F \\ \dot{\theta}_F \\ \dot{\psi}_F \end{pmatrix} \tag{12}$$

where the subscript F indicates the body axis system. The matrix R_{FT} represents the transformation of the body axis system to the Earth-fixed axis system. This matrix defines the aircraft trim attitude with respect to earth axis and is given by:

$$R_{FT} = \begin{bmatrix} 1 & 0 & -\sin\theta_{FT} \\ 0 & \cos\phi_{FT} & \sin\phi_{FT}\cos\theta_{FT} \\ 0 & -\sin\phi_{FT} & \cos\phi_{FT}\cos\theta_{FT} \end{bmatrix} \tag{13}$$

where θ_{FT} and ϕ_{FT} are the trim Euler angles for rigid body pitch and roll. The trim Euler angles are obtained from the CAMRAD/JA trim solution and are dependent upon the flight conditions.

The linear and angular displacement perturbation vectors of a point P are therefore given by:

$$u_p = u_{cg} + \begin{pmatrix} \phi_F \\ \theta_F \\ \psi_F \end{pmatrix} \times r_{cg,p}$$

$$\underset{\text{Eqn. (12)}}{=} u_{cg} - (r_{cg,p} \times) R_{FT} \begin{pmatrix} q_1 \\ q_2 \\ q_3 \end{pmatrix} \tag{14}$$

and

$$\theta_p = \begin{pmatrix} \phi_F \\ \theta_F \\ \psi_F \end{pmatrix} = R_{FT} \begin{pmatrix} q_1 \\ q_2 \\ q_3 \end{pmatrix} \tag{15}$$

where $r_{cg,p}$ is the position vector of point P relative to the center of gravity in the body axis system, ψ_{FT} is the perturbation rigid body trim Euler angle for yaw, and $\times$ indicates a vector cross-product.

Therefore the mode shapes for the rigid body motion are:

$$[\xi_1 \ldots \xi_6] = [\, (-r_{cg,p} \times) R_{FT} \quad \mathbf{I} \,] \tag{16}$$

$$[\gamma_1 \ldots \gamma_6] = [\, R_{FT} \quad \mathbf{0}] \tag{17}$$

where $\mathbf{I}$ represent a 3x3 diagonal unit matrix and $\mathbf{0}$ represent a 3x3 zero matrix.

The total velocity of point P in the body axis system is the sum of the trim velocity, V_{trim}, and perturbation velocities:

$$\dot{u}_p = V_{trim} + \sum_{k=1}^{\infty} \dot{q}_k \xi_k \tag{18}$$

The components of V_{trim} in the x-, y-, and z-directions are obtained from the CAMRAD/JA trim solution. The acceleration of point P is the sum of the perturbation accelerations and the inertial acceleration due to the rotation of the trim velocity vector by the body axes angular velocity. Therefore in the body axis system:

$$\ddot{u}_p = \omega_F \times V_{trim} + \sum_{k=1}^{\infty} \ddot{q}_k \xi_k$$

$$\underset{\text{Eqn. (12)}}{=} (-V_{trim} \times) \begin{pmatrix} \dot{q}_1 \\ \dot{q}_2 \\ \dot{q}_3 \end{pmatrix} + \sum_{k=1}^{\infty} \ddot{q}_k \xi_k \tag{19}$$

Equations (14)-(15), (18), and (19) describe the three components of the displacement, velocity, and acceleration of point P, respectively, in the aircraft body axis system.

A separate axis system is defined as being attached to the sensor at airframe location P. If the orientation of this sensor axis system does not coincide with the body axis system the displacement vector u_P, velocity vector $\dot{u}_P$, and acceleration vector $\ddot{u}_P$ need to be transformed into the sensor axis system by consecutive rotations of the vector around the body z-axis, the new y-axis, and the resulting x-axis. The components of the motion vector in the sensor axis system are used to define the elements of j^{th} row of the sensor matrices C_i (i=0,1,2), which in turn define the output of a single-direction motion sensor at point P, represented by the j^{th} element of the sensor vector y.

TIME RESPONSE

The time history response of the linear system of Eqn. (8) is given by[16]:

$$x_S(t) = e^{A(t-t_0)}x_S(t_0) + \int_{t_0}^{t} e^{A(t-\tau)}Bv(\tau)d\tau \qquad (20)$$

If the system matrix A has distinct eigenvectors the exponential power e^{At} can be rewritten as:

$$e^{At} = Me^{(M^{-1}AM)t}M^{-1} \qquad (21)$$

where M is a matrix of linearly independent eigenvectors. The columns of matrix M, the so-called modal matrix, are made up of the eigenvectors with columns corresponding to the eigenvalues λ_i of matrix A. The matrix manipulation $M^{-1}AM$ results in the transformation of A into the diagonal eigenvalue matrix Λ. Thus, Eqn. (20) can be rewritten as:

$$x_S(t) = Me^{\Lambda(t-t_0)}M^{-1}x_S(t_0) + \int_{t_0}^{t} Me^{\Lambda(t-\tau)}M^{-1}Bv(\tau)d\tau \qquad (22)$$

For a given constant coefficient system, the modal matrix, its inverse, and the control matrix B are constant coefficient matrices. If it is assumed that the control vector v(t) (Eqn. (2)) is constant over the considered time period from t_0 to t, then Eqn. (22) can be rewritten as:

$$x_S(t) = Me^{\Lambda(t-t_0)}M^{-1}x_S(t_0) + M\left(\int_{t_0}^{t} e^{\Lambda(t-\tau)}d\tau\right)M^{-1}Bv \qquad (23)$$

As previously discussed the system control input v(t) is defined as:

$$v(t)=v_p(t)+v_{ac}(t) \qquad (2)$$

If the control input v(t) is digitized at time step intervals of Δt and the assumption is made that the control input is constant over the time step Δt, i.e. $v(t)=v(t_i)$ for $t_i < t < t_i+\Delta t$, then the system response x_S at time $t_i+\Delta t$ can be calculated from the system state at time t_i, $x_S(t_i)$, and the system response to a step input of magnitude $v(t_i)$ at time t_i by using Eqn. (23).

$$x_S(t_i+\Delta t) = Me^{\Lambda\Delta t}M^{-1}x_S(t_i) + M\int_{t_i}^{t_i+\Delta t} e^{\Lambda(t_i-t)}d\tau M^{-1}Bv(t_i) \qquad (24)$$

or in matrix form:

$$x_S(t_i+\Delta t) = Me^{\Lambda\Delta t}M^{-1}x_S(t_i) + \Lambda^{-1}M\{e^{\Lambda\Delta t} - I\}M^{-1}Bv(t_i) \qquad (25)$$

where I is the diagonal unit matrix.

The response $x_S(t_i)$ in Eqn. (24) represents the state of the system at time t_i. The state velocities $\dot{x}_S(t_i)$ are obtained from Eqn. (8). Knowledge of the first order state variables x_S and $\dot{x}_S$ at time t_i allows the extraction of the displacements x, the velocities $\dot{x}$, and the accelerations $\ddot{x}$ of the aircraft degrees of freedom in Eqn. (1). The sensor vector y can then be calculated from Eqn. (2) and the active control input v_{ac} from Eqn. (3). The input v to the system at time step $(t_i+\Delta t)$ is set equal to (Eqn. (2)):

$$v(t_i+\Delta t) = v_p(t_i+\Delta t) + v_{ac}(t_i) \qquad (26)$$

NOISE

To account for instrumentation signal noise and/or for sensor modelling uncertainty within the sensor model, noise can be simulated by rewriting the sensor vector, y (Eqn. (3)):

$$y(t_i) = C_2\ddot{x}(t_i) + C_1\dot{x}(t_i) + C_0x(t_i) + D_0v(t_i) + w(t_i) \qquad (27)$$

where $w(t_i)$ is a vector representing sensor noise. For this study the sensor noise is defined as:

$$w(t_i) = rg_m, \quad -1.0 \leq r \leq +1.0 \qquad (28)$$

where r is a random number and g_m defines the sensor noise level or magnitude.

AIRCRAFT MODEL

An XV-15 size joined-wing tilt-rotor aircraft (model 166CL in Ref. 2) in cruise flight was considered for this investigation. The aircraft has a three-bladed, 25-foot diameter, gimbal-mounted, stiff-inplane proprotor. Table 2 provides a description of the key geometric parameters for the rotor and the airframe as obtained from Ref. 2 and 17.

The airframe structural characteristics, consisting of the modal frequency and mass and of the hub motion due to elastic airframe deformation for the joined-wing tilt-rotor aircraft were reported in Ref. 2 for six airframe mode shapes, representing three symmetric and three anti-symmetric modes. Table 3 provides these data for the six elastic airframe degrees of freedom. This mode shape information at the hub location is used in the CAMRAD/JA code, which provided the mathematical plant model of the joined-wing tilt-rotor aircraft. Table 4 presents the location of the aircraft center of gravity and the rotor hubs for the aircraft.

RESULTS

The following degrees of freedom were included in the present investigation: six rigid-body degrees of freedom, six (three symmetric and three anti-symmetric) elastic airframe modes, two rotor blade bending and one rotor blade torsion mode, the hub gimbal, and rotor speed degrees of freedom. The plant model, as calculated by CAMRAD/JA, consisted of the system matrices A_i (i=0,1,2) and the control matrix B_0 for both symmetric and anti-symmetric flight modes. Both the symmetric and anti-symmetric plant models consisted of eighteen degrees of freedom per flight mode: three rigid and three elastic body modes; the flap, chord, and torsion modes for each rotor blade, resulting in nine rotor modes for the three bladed rotor; two hub gimbal and one rotor speed. Structural damping was set at 3 percent of critical damping for the rotor modes and 2 percent critical damping for the elastic airframe modes. The airframe aerodynamic damping was assumed zero. The control vector, v, consisted of the collective pitch and the lateral and longitudinal cyclic pitch.

STABILITY OF AIRCRAFT WITHOUT FEEDBACK

This section will discuss the results of the stability analysis for the basic aircraft, i.e., the joined-wing tilt-rotor aircraft without feedback control. The CAMRAD/JA code was used to obtain the mathematical plant model of the basic tilt-rotor aircraft in cruise as given by Eqn. (1) for a forward flight range from 150 to 350 knots at standard sea level conditions. For a tilt-rotor aircraft configuration in cruise flight the CAMRAD/JA analysis divides the aircraft motion into uncoupled symmetric and anti-symmetric flight modes. Separate system matrices, A_i (i=0,1,2) and B_0, are calculated for each flight mode. The system matrices for a selected flight mode and flight trim condition formed the input to the analysis code, which used an eigenvalue analysis to evaluate the stability of the aircraft without the application of active controls.

Figure 6 presents the results of the stability analysis for the basic joined-wing tilt-rotor aircraft in the form of root-locus plots for both the symmetric (Figs. 6a and 6b) and anti-symmetric (Figs. 6c and 6d) flight modes. The natural frequency and damping ratio for the three wing modes were calculated and are shown in Figs. 7 and 8 for the symmetric and anti-symmetric flight modes, respectively. Wing modes 1s and 1a are the critical modes for the symmetric and anti-symmetric flight modes, respectively. The symmetric flight modes shows a whirl-flutter velocity of approximately 243 knots, while for the anti-symmetric flight modes the occurrence of whirl-flutter occurs at the higher flight speed of approximately 275 knots. Reference 2 reports a flutter speed of approximately 240 and 250 knots for the symmetric and anti-symmetric flight modes, respectively. The discrepancy between the results of the present investigation and of Ref. 2 for the anti-symmetric flight mode flutter speed is not understood.

CLOSED LOOP RESULTS - State Variable Domain

As noted in the previous section the onset of whirl-flutter occurred in the symmetric flight mode first and therefore the emphasis in the present investigation was towards determining the feasibility of using active controls to increase the flutter velocity for this flight condition. The flight velocity of 275 knots was

selected as the flight condition for evaluation of various active control schemes.

Accelerometers were considered to be the preferred sensor to be used in the feedback system. Because of the availability of rotor cyclic pitch control on the tilt-rotor aircraft in cruise flight it was decided to use the cyclic pitch as the active control input v_{ac}. References 10 and 11 also used the closed-loop, cyclic pitch control to improve the whirl-flutter stability of the cantilever-wing tilt-rotor models.

The feasibility of whirl-flutter alleviation through active controls was first investigated in the state space domain. Only state variable accelerations were used in the sensor model. The matrices C_1, C_0, and D_0 in Eqn. (3) were zero matrices, while the C_2 matrix elements had the value of "1" or "0", depending upon whether a particular state variable acceleration was incorporated into the closed-loop feedback system.

Since the first wing mode, $q_{w,1s}$, was the critical mode for the onset of whirl-flutter, the acceleration for this state variable was selected for the sensor output and the longitudinal cyclic pitch, δ_s, and lateral cyclic pitch, δ_c, were selected for possible active control inputs.

Figure 9 presents the effect of various longitudinal cyclic pitch feedback gains on the stability of the elastic wing mode 1s at 275 knots. A positive feedback gain for $\ddot{q}_{w,1s}/\delta_s$ has the desired stabilizing effect on the wing mode 1s, has little effect on wing mode 3s, but has a destabilizing effect on wing mode 2s. Figure 10 shows the effect of lateral cyclic pitch feedback on the frequency and damping ratio of wing modes 1s, 2s, and 3s at 275 knots. A negative feedback gain for $\ddot{q}_{w,1s}/\delta_c$ has a stabilizing effect on wing mode 1s, while having a destabilizing effect on wing modes 2s and 3s. Figures 9b and 10b show that all three wing modes will be stable for $1.6<\ddot{q}_{w,1s}/\delta_s<4.0$ g/rad or $\ddot{q}_{w,1s}/\delta_c<-2.5$ g/rad.

It should be noted here that feeding back the wing mode 1s acceleration as described above also influences the frequency and damping of other body and rotor degrees of freedom, i.e., their eigenvalue location in the root locus plot changes. One rotor mode, a rotor lead/lag bending mode, was significantly influenced by the feedback of wing mode 1s acceleration, $\ddot{q}_{w,1s}$, to either the longitudinal or lateral cyclic pitch. This sensitivity is shown in Fig. 11. From comparison of Figs. 9b and 11b it is seen that at the feedback gain values of $1.6<\ddot{q}_{w,1s}/\delta_s<4.0$ g/rad where the wing mode 1s is damped this critical rotor mode has become unstable. Comparison of Figs. 10b and 11b shows that this rotor mode has also become unstable at feedback gain values for $\ddot{q}_{w,1s}/\delta_c<-2.5$ g/rad, which is the desired gain level to stabilize wing mode 1s. Figure 11b shows that the magnitude of negative damping ratio for the critical rotor mode is slightly lower for the required feedback gain levels for $\ddot{q}_{w,1s}/\delta_s$ as compared to the required feedback gain levels for $\ddot{q}_{w,1s}/\delta_c$ to stabilize the wing mode 1s. Therefore the longitudinal cyclic pitch, δ_s, was selected as the active control input.

An obvious choice to stabilize the system is the additional feedback of the critical lead/lag mode to cyclic pitch. A sensitivity analysis showed, however, that this critical rotor mode could be influenced by feedback of wing modes 2s and 3s to either longitudinal or lateral cyclic pitch. Again the longitudinal cyclic pitch, δ_s, was selected at the active control input for feedback of wing modes 2s and 3s.

As this study was a preliminary investigation into the use of active controls for whirl-flutter alleviation, no effort was made to optimize the feedback control system. A number of combinations of $\ddot{q}_{w,1s}/\delta_s$, $\ddot{q}_{w,2s}/\delta_s$, and $\ddot{q}_{w,3s}/\delta_s$ gain values were evaluated using the closed-loop analysis code until a stable system (including rotor stability) was obtained for the desired condition of 275 knots flight velocity. Satisfactorily stability was obtained for a closed-loop system using a $\ddot{q}_{w,1s}/\delta_s$ gain of 2.0 g/rad and a $\ddot{q}_{w,3s}/\delta_s$ gain of -1.25 g/rad. The effect of flight velocity on the stability of this closed-loop symmetric flight mode system is shown in Fig. 12. The natural frequencies and damping ratios for the three wing modes for both the basic aircraft and the closed-loop system are shown. Little effect of using this type of active control on the natural frequency of these wing modes is observed (Fig. 12a). However, the damping ratio of all three wing modes is changed substantially (Fig. 12b). Wing mode 1s shows more damping, while wing modes 2s and 3s show reduced damping from the configuration with no feedback control. Figure 12 shows that even non-optimal feedback in the state domain of wing chord and wing torsional accelerations to longitudinal cyclic pitch can increase the tilt-rotor whirl-flutter speed from 243 to above 275 knots, a 13.2% improvement in the flutter velocity.

CLOSED LOOP RESULTS - Physical Domain

The previous section showed that feedback of state variable accelerations to cyclic pitch can be used to delay the onset of whirl-flutter on the joined-wing tilt-rotor aircraft. However, to be able to feed back pure state variables requires the identification of the individual system modes which would potentially require a large number of sensors mounted on the aircraft. Flutter alleviation studies on fixed-wing aircraft have shown that it is possible to increase the aircraft flutter velocity by feeding back the output of a limited number of accelerometers mounted at appropriate locations near the wing tip to an active control input, such as a wing control surface[18,19]. The use of a limited number of accelerometers mounted at appropriate locations near the wing tip, whose signal output is then fed back to a blade pitch control was studied in Ref. 11 for a cantilever-wing tilt-rotor aircraft configuration to increase the whirl flutter speed from 285 to above 300 knots. Use of a limited number of wing mounted accelerometers was also investigated here for the joined-wing tilt-rotor aircraft. Again the rotor longitudinal cyclic pitch was selected for the active control input.

The results of the state variable domain analysis discussed in the previous section showed that the feedback of the accelerations of the wing modes 1s and 3s degrees of freedom to longitudinal cyclic pitch could be used to stabilize the joined-wing tilt-rotor aircraft at 275 knots flight speed. It was therefore decided to use wing-mounted, single-direction accelerometers which would measure these two aircraft degrees of freedom as the sensors in the feedback system. Only the symmetrical flight mode was analyzed in the "physical" domain. In application, wing-mounted sensors would also measure the acceleration due to the anti-symmetric wing elastic deformations and anti-symmetric rigid body motion. However, by placing sensors in the same location on opposite wings and by summing the corresponding sensor output signals the contribution of these anti-symmetric flight modes could be eliminated.

As mentioned earlier, Ref. 2 only provided the elastic airframe mode shape information for the rotor hub location. Therefore hub–mounted accelerometers, which provide hub accelerations in the body axis system were considered here. Reference 11 showed that the location of the wing-mounted sensors can be an important parameter in the closed loop active control system to increase the whirl flutter velocity on a tilt-rotor aircraft. Therefore the hub location is not necessarily the best location for the closed-loop system sensors.

The airframe modal information for the hub location together with the CAMRAD/JA calculated trim information (the cruise velocity vector V_{trim} and the trim Euler angles ϕ_{FT} and θ_{FT}, Eqn. 11) were input to the sensor model utility (Fig. 4). This utility then determined the contribution of each aircraft degree of freedom to the hub accelerations in body x-, y-, and z-directions. The assumption was made that the contribution of the symmetric rigid body motion to the acceleration at the hub (Eqn. (17)) was eliminated by means of a high pass filter. Mathematically this equates to setting the corresponding C_i-matrix elements to zero. As mentioned previously, no attempt was made to model the dynamics of the swashplate actuators in the mathematical description of the feedback control system. The 275-knot flight trim condition was again selected for the evaluation of the various feedback control schemes.

Table 3 shows that for wing mode 1s the linear displacement in vertical direction is an order of magnitude higher than the linear displacements in both the chord-wise and span-wise directions. A single-direction, hub-mounted accelerometer with its sensing direction along the body z-axis was therefore selected for the measurement of the wing mode 1s degree of freedom. As was expected from the results of the state domain analysis, negative feedback of the hub vertical acceleration, $\ddot{u}_{h,v}$, to the longitudinal cyclic pitch, δ_s, also adversely affected the stability of the critical rotor lead/lag mode (at 2.3/rev) as seen in Fig. 13a. A sensitivity analysis showed that this adverse effect could be reduced by eliminating the contributions of wing modes 2s and 3s to the hub vertical acceleration measurement as can be seen from comparison of Figs. 13a and 13b. Physically this could be accomplished be means of a notch filter on the accelerometer output signal. Mathematically the effect of the notch filter was simulated by setting the C_2-elements' corresponding to the mode 2s and 3s contributions to zero. Eliminating the wing mode 2s and 3s contributions also reduces the effect of the $\ddot{u}_{h,v}/\delta_s$ feedback on the damping ratios of these two wing modes as seen from comparison of Figs. 13a and 13b.

A sensitivity analysis showed that feeding back the hub acceleration in wing chord-wise direction, $\ddot{u}_{h,c}$, and in wing span-wise direction, $\ddot{u}_{h,s}$, to longitudinal cyclic pitch, δ_s, had a stabilizing effect on the critical rotor mode as shown in Figs. 14a and 14b, respectively. A

slight beneficial effect of such feedback on the 1s wing mode damping ratio is also observed in Figs. 14a and 14b, although the mode remains unstable.

A feedback system was selected consisting of two hub accelerometers measuring vertical and span-wise hub accelerations, whose outputs were fed back to the longitudinal cyclic pitch. The hub vertical acceleration measurement was assumed to be conditioned by means of a notch filter so as to eliminate the contribution of wing modes 2s and 3s from this sensor output signal. As mentioned before a high pass filter was also used to eliminate the contributions of the rigid body modes to the measured hub accelerations. This feedback system was analyzed in the following manner. The value of the feedback control gain $\ddot{u}_{h,v}/\delta_s$ was fixed while the feedback gain $\ddot{u}_{h,s}/\delta_s$ was varied systematically within the closed-loop analysis code. After each $\ddot{u}_{h,s}/\delta_s$ change the code performed an eigenvalue analysis to determine the stability of the closed-loop system. This process was then repeated for different $\ddot{u}_{h,v}/\delta_s$ values.

Feedback of hub vertical acceleration $\ddot{u}_{h,v}$ (gain=0.0048g/rad, with a notch filter on the sensor output signal), and hub span-wise acceleration $\ddot{u}_{h,s}$, (gain=-0.0035g/rad) to the longitudinal cyclic pitch produced a stable closed-loop system. This feedback system was analyzed over the tilt-rotor aircraft velocity range from 150 to 350 knots. Figure 15 compares the stability of the three wing modes for the basic joined-wing tilt-rotor aircraft (no feedback) and for the closed-loop system. Little effect on wing natural frequencies is found (Fig. 15a). The effect of flight speed on the damping for the closed-loop system is shown in Fig. 15b. Comparison of Fig. 15b with the results obtained for the state variable domain analysis (Fig. 12b) shows similar results for the damping ratio for the critical wing mode 1s. Lower damping ratio values are observed for wing mode 2s for the closed-loop "physical" domain analysis (Fig. 15b) when compared to the state variable domain results (Fig. 12b). A large decrease in the wing mode 3s damping ratio was seen in Fig. 12b for the closed-loop system as compared to the no feedback case. In contrast, Fig. 15b shows very little influence of the "physical" domain closed-loop feedback system on the wing mode 3s damping ratio. Figure 15 illustrates that again a 13.2% increase in the whirl-flutter velocity from 243 to 275 knots was obtained.

Figure 16 shows the root locus plot for this closed-loop system for the speed range from 150 to 350 knots. Comparison of the root locus plots of Fig. 6 (basic aircraft without feedback control) with Fig. 16 (closed-loop system) also shows the improved stability for the closed-loop system, but at the same time illustrates the effect of the feedback system on the damping of the various rotor and aircraft degrees of freedom. The rotor lead/lag mode at 2.3/rev shows an decrease in damping due to the hub acceleration feedback system and is neutrally stable at approximately 278 knots. Little effect on the other rotor modes and on the rigid body modes is observed.

TIME RESPONSE CALCULATIONS:

To evaluate the magnitude of the required active control input, the time response of the aircraft at a 270-knot cruise condition was calculated. Time-history response calculations were made for both the basic aircraft (no feedback control) and for the closed-loop system. A longitudinal cyclic pitch control input, v_p (Eqn. (2)), representing a square doublet with a 1.0 deg magnitude and a period of 1.0 sec (Fig. 17a) was used to excite the system at this 270-knot trim condition. The calculated sensor response for the two accelerometers at the rotor hub is presented in Figs. 17b and 17c for the basic aircraft. The response of the higher aircraft modes results in the higher frequency response in the accelerometer output (Figs. 17b and 17c) during the first 1-1.5 sec (approximate 12 rotor revolutions) of the motion. A rapid divergence of the vertical acceleration magnitude is observed (Fig. 17c). The acceleration in the vertical direction is approximately a factor 5 higher than the measured span-wise acceleration (Fig. 17c vs. Fig. 17b).

The time response of the closed-loop system to the same square doublet is shown in Fig. 18 for the first 2 seconds and in Fig. 19 for the first 15 seconds, which equates to approximately 115 rotor revolutions. The closed-loop system (Fig. 18b) shows slightly higher span-wise accelerations during the first 2 seconds of the response as compared to the basic aircraft time response (Fig. 17b). The vertical accelerations for the closed-loop system (Fig. 18c) are 50% lower than those observed for the basic aircraft (Fig. 17c) during this 2 second period. Figure 19 shows that after 15 seconds (115 rotor revolutions) the aircraft has not yet reached a steady-state condition. The measured accelerations in vertical and span-wise direction after 15 seconds are approximately one-third (0.5g's and 0.2g's, respectively) the maximum value experienced due to the doublet excitation (1.9g's and 0.7g's, respectively).

After 10-12 seconds the hub vertical acceleration measurement shows a single frequency content of 3.6 Hz. This corresponds to the first wing mode (mode 1s). The time response signal for the span-wise accelerometer is presented in Figs. 18b and 19b and shows a multiple frequency content throughout the 15 seconds of the calculated aircraft time response. Again a higher frequency response is observed in the accelerometer outputs (Figs. 18b and 18c), which is similar in character to the sensor output of the basic aircraft (Figs. 17b and 17c) during the first 1.5 seconds. It is believed that the higher frequency content during the first few seconds is a basic aircraft behavior and is not the result of the feedback system. However, the influence of these higher frequencies on the measured signal persist for approximately 10 seconds (Figs. 19b and 19c), and it is thought that the strong coupling of the rotor lead/lag mode at 2.3/rev with the first wing mode (1s) within the closed-loop system is the main cause of the longer time period for the higher frequency influence to damp out.

The longitudinal cyclic pitch active control input is shown in Figs. 18a and 19a. A maximum active control input of 0.009 deg is observed. The 0.009 deg cyclic pitch input equates to a rotor active control force of approximately 9 lbs being applied at the rotor hub to damp the wing motion and to delay the tilt-rotor whirl-flutter instability. This level of active control input for the longitudinal cyclic pitch is of the same magnitude as that predicted by the author for a similar flutter alleviation study for a cantilever-wing tilt-rotor aircraft configuration[11] and is a major improvement over the levels of cyclic pitch control predicted by Nasu[7], who showed a required cyclic pitch control angle of 0.5 deg. The higher frequency content can also be observed in the active longitudinal cyclic control input in Fig. 18a and in Fig. 19a for the first 10 seconds of the motion. After 10-12 seconds the active control input shows the single frequency content of 3.6 Hz, corresponding to the critical wing mode 1s.

For the actual vehicle it is unlikely that actuators can be accurately controlled for 0.009 deg of pitch input. Control system dynamics (actuators, swashplate, hydraulic system,...) will have to be included in the simulation to achieve more realistic results. However, these results provide two important findings. First, the level of hub force generation necessary to stabilize the tilt-rotor is very small and can be easily withstood without adverse dynamic loads or degrading aircraft handling quality characteristics. Second, the frequency requirements for the control actuators are within the bandwidth of current electro-hydraulic actuation flight hardware.

The closed-loop system response to a square doublet was also calculated for two cases where the sensor signals were contaminated by noise, representing signal instrumentation noise and/or uncertainty regarding the accuracy of the system modeling. Based upon the time response calculations shown in Fig. 19, noise gain levels for g_m (Eqn. (28)) of 0.1 and 0.5 were selected. This represents a noise level of 0.1 g and 0.5g, respectively, for the two hub-mounted accelerometers. The corresponding time responses for the closed-loop system are shown in Figs. 20 and 21, respectively. Comparison of Fig. 19 (no noise) with Fig. 20 (0.1g noise) shows essentially the same time response behavior with the noise contamination. Figure 21a shows that the 0.5g sensor noise contamination level causes an increase in the required level of active longitudinal cyclic pitch control from 0.009 deg (no noise) to 0.010 deg for the first few seconds after disturbing the system. After 10 seconds an increase in the required magnitude of the active control level from 0.0025-0.0030 deg for the no-noise case (Fig. 19a) to approximately 0.005 deg for the 0.5g noise case is observed (Fig. 21a). The periodic character of the active control is not readily observable in Fig. 21a. A decrease in the magnitude of the hub horizontal and vertical accelerations over time is seen (Figs. 21b and 21c). The observed response decay rate for the 0.5g noise case (Fig. 21) is smaller than the decay rates observed for the no-noise (Fig. 19) and 0.1g noise (Fig. 20) cases. However, the closed-loop system with 0.5g noise contamination on the sensors, representing 25% of the maximum observed sensor response level of 2.0g vertical hub acceleration, still shows a stable system indicating a robust control system.

CONCLUSIONS

The present investigation showed that it is possible to delay the onset of whirl-flutter on a XV-15 size joined-wing tilt-rotor aircraft through the use of active controls. The CAMRAD/JA code was used to obtain a set of linear differential equations, which describe the motion of the tilt-rotor aircraft in cruise. The airframe vibration mode shapes, modal frequencies, and modal masses for a representative joined-wing tilt-rotor aircraft were used. The CAMRAD/JA output, consisting of the open-loop system matrices, and a sensor

model utility output were input to a separate program, which performed the closed-loop, active control calculations. An eigenvalue analysis was performed to determine the flutter stability of both open- and closed-loop systems.

- Sensor models based upon the feedback of pure state variables increased the whirl-flutter velocity from 243 to over 275 knots by feeding back the first and third wing elastic bending degrees of freedom to the longitudinal cyclic pitch.
- Whirl-flutter could also be delayed from 243 to above 275 knots by feeding back hub span-wise and vertical accelerations to the longitudinal cyclic pitch.
- Time response calculations at a 270-knot cruise condition showed an active cyclic pitch control level of 0.009 deg, which equates to a very acceptable 9 pound active control force applied at the rotor hub.
- Contamination of the sensor output signal with noise, whose magnitude was equal to 25% of the maximum measured amplitude of the sensor output did not adversely effect the closed-loop system stability, indicating a robust control system.

REFERENCES

[1]Felker, F.F., and Light, J.S., "Aerodynamic Interactions Between a Wing and a Rotor in Hover", Journal of the American Helicopter Society, Vol. 33, No. 2, April 1988.

[2]Wolkovitch, J., Wainfan, B., Yitzhak, B.H., and Johnson, W., "Application of the Joined Wing to Tiltrotor Aircraft", NASA CR-177543, November 1989.

[3]Wolkovitch, J., "The Joined Wing: An Overview", Journal of Aircraft, Vol. 23, No. 3, March 1986,.

[4]Ham, N.D., and Whitaker, H.P., "A Wind-Tunnel Investigation of Tilt-Rotor Gust Alleviation Systems," NASA CR-152264, January 1978.

[5]Ham, N.D., Bauer, P.H., Lawrence, T.H., and Yasue, M., "A Study of Gust and Control Response of Model Rotor-Propellers in a Wind Tunnel Airstream," NASA CR-137756, August 1975.

[6]Frick, J., and Johnson, W., "Optimal Control Theory Investigation of Proprotor/Wing Response to Vertical Gust," NASA TMX-62384, September 1974.

[7]Jenie, S.D., "The Application of Active Control Technology to a Gust Alleviation System for the Tilt-Rotor Aircraft with Hingeless Rotors," NASA CR-152173, February 1978.

8Miller, D.G., and Ham, N.D., "Active Control of Tilt-Rotor Blade In-Plane Loads During Maneuvers," Proceedings of the Fourteenth European Rotorcraft Forum, Milan, Italy, September 1988.

[9]Straub, F.K., and Warmbrodt, W., "The Use of Active Controls to Augment Rotor/Fuselage Stability," Journal of the American Helicopter Society, Vol. 30, No. 3, July 1985.

[10]Nasu, K., "Tilt-Rotor Flutter Control in Cruise Flight," NASA TM 88315, December 1986.

[11]van Aken, J.M. "Alleviation of Whirl-Flutter on Tilt-Rotor Aircraft Using Active Controls," Proceedings of the 47th Annual Forum of the American Helicopter Society., Phoenix, Az, May 1991.

[12]Johnson, W., "A Comprehensive Analytical Model of Rotorcraft Aerodynamics and Dynamics, Part I: Analysis Development", NASA TM 81182, June 1980.

[13]Johnson, W., "Development of a Comprehensive Analysis for Rotorcraft - I, Rotor Model and Wake Analysis," Vertica, Vol. 5, No. 2, 1981.

[14]Johnson, W., "Development of a Comprehensive Analysis for Rotorcraft - II, Aircraft Model, Solution Procedures and Applications," Vertica, Vol. 5, No. 3, 1981.

[15]Johnson, W., "A Comprehensive Analytical Model of Rotorcraft Aerodynamics and Dynamics, Johnson Aeronautics Version", Johnson Aeronautics, Palo Alto, CA, 1988.

[16]Ogata, K., State Space Analysis of Control Systems, Prentice-Hall, Inc., NJ, 1967.

[17]Maisel, M, "Tilt Rotor Research Aircraft Familiarization Document," NASA TM X-62,407, January 1975.

[18]Sanford, M.C, Abel, I, and Gray, D.L., "Development and Demonstration of a Flutter-Suppression System Using Active Controls", NASA TR R-450, April 1975.

[19]Newsom, J.R., Abel, I., and Dunn, H.J., "Application of Two Design Methods for Active Flutter Suppression and Wind-Tunnel Test Results", NASA TP 1653, May 1980

Appendix A: Comprehensive Rotorcraft Analysis

CAMRAD/JA (for Comprehensive Analytical Model of Rotorcraft Aerodynamics and Dynamics, Johnson Aeronautics version) is an analysis designed to calculate rotor performance, aerodynamic and structural loads, aircraft vibration, gust response, flight dynamics, handling qualities, and aeroelastic stability. The analysis development is discussed in detail in References 12-15.

The rotor aerodynamic model is based on lifting-line theory, and uses two-dimensional airfoil characteristics, and a vortex wake. For the

aeroelastic stability analysis it is generally sufficient to use the uniform inflow model of CAMRAD/JA, i.e. assuming a linear variation of inflow over the rotor disk. The rotor structural model is based on engineering beam theory for rotating wings with large pitch and pretwist. Both rigid and elastic blade motion are included. A modal method is used to calculate, in vacuum, the blade bending modes for the rotor. Blade torsion modes are not coupled with the bending modes, but are calculated independently. The total elastic rotor response is a linear combination of the modal solution in which the bending and torsion motion of the rotor are coupled.

An orthogonal mode representation of the body elastic motion is used in CAMRAD/JA. The airframe structural vibration modes need to be obtained from a separate structural analysis (in the present analysis the MSC-PAL finite element structural analysis code was used). The linearized equations of motion for the rigid body degrees of freedom are used in the calculation of the aircraft vibration and transition motion. For this study the aerodynamic forces on the wing-body, horizontal tail and vertical tail are modelled, including control surfaces. Static aircraft aerodynamic characteristics were obtained from a wind tunnel test. The generalized aerodynamic damping and control forces on the airframe elastic modes can be included in CAMRAD/JA and these terms are normally estimated for the frequency of the principal excitation of the mode. In the present analysis these dampings were set to zero. The airframe aerodynamic representation is basically a quasi-static model.

The aircraft motion consists of the six rigid-body degrees of freedom and the elastic free vibration body modes. A body-axis coordinate frame with origin at the aircraft center of gravity is used for the description of the motion. For the elastic motion of the aircraft in flight, the displacement and rotation at an arbitrary point are expanded in a series of the orthogonal free vibration modes. The first six degrees of freedom for the elastic aircraft motion at this arbitrary point are the rigid body motions, while the remaining body degrees of freedom represent the elastic modes of the aircraft. (See the sensor model derivation in the main text).

The rotor equations of motion require the six components of the hub linear and angular motion in the shaft axis system due to both the rigid and elastic aircraft body motion. This information was obtained from the results of the MSC-PAL analysis as reported in Ref. 2 (see table 3).

CAMRAD/JA first performs the trim analysis, in which the equations of motion are solved for the case of a steady state flight condition. Aeroelastic stability is then calculated from the trim solution by constructing the system matrices that describe the linear differential equations of motion and performing an eigenvalue analysis.

Table 1: Comparison of tilt-rotor model of Refs. 10 and 11 with present investigation.

Nasu (Ref. 10)	van Aken (Ref. 11)	Present investigation
Cantilever-wing model	Cantilever-wing aircraft	Joined-wing aircraft
Semi-span wing model: no rigid body motion symmetric flight mode	Free flight: rigid body motion symmetric and anti-symmetric flight modes	Free flight: rigid body motion symmetric and anti-symmetric flight modes
Elastic body modes: symmetric modes only wing chordwise bending wing beamwise bending wing torsion	Elastic body modes: symmetric and anti-symmetric wing chordwise bending wing beamwise bending wing torsion pylon yaw	Elastic body modes: symmetric and anti-symmetric wing mode 1 wing mode 2 wing mode 3
Rotor: 3 bladed hingeless rotor blade chordwise bending blade beamwise bending	Rotor: 3 bladed hingeless rotor blade chordwise bending blade beamwise bending blade torsion rotor speed gimbal motion	Rotor: 3 bladed hingeless rotor blade chordwise bending blade beamwise bending blade torsion rotor speed gimbal motion
Feedback system: using state variables	Feedback system: using state variables using wing mounted accelerometers	Feedback system: using state variables using hub mounted accelerometers

Table 2: Specifications of joined-wing tilt-rotor aircraft model

Rotor:	
number of blades	3
blade radius	12.5 ft
solidity, σ	0.0890
airfoil section	64-series
rotational speed	458 rpm
shaft cant angle	-1 deg.
mast height	4.667 ft
Wing:	
semispan	16.1 ft
forward wing:	
chord	3.5 ft
sweep (forward)	6.5 deg
airfoil thickness	12%
aft wing:	
chord	1.7 ft
sweep (forward)	15 deg
airfoil thickness	12%
airfoil section	64A212
Aircraft weight	13,000 lbs

Table 3: Wing mode shape information at right hub

symmetric modes	mode 1s	mode 2s	mode 3s
frequency, Hz	3.65	5.56	7.30
modal mass, slug/12	1.833	0.832	0.375
linear displacements:			
x, in	-0.0735	0.1265	0.0341
y, in	0.0771	-0.1318	-0.0340
z, in	-0.4530	-0.1439	-0.0655
angular displacements:			
x, rad.	-0.00313	-0.00001	0.0015
y, rad.	0.00515	0.00400	0.00178
z, rad.	0.0011	-0.00199	-0.00049

anti-symmetric modes	mode 1a	mode 2a	mode 3a
frequency, Hz	4.75	7.42	8.13
modal mass, slug/12	0.639	0.393	1.295
linear displacements:			
x, in	-0.0025	0.0324	0.1576
y, in	-0.0089	-0.0104	-0.1706
z, in	0.2578	-0.0841	0.0339
angular displacements:			
x, rad.	0.0011	0.0017	0.0010
y, rad.	-0.0053	0.00253	-0.0006
z, rad.	0.0001	-0.00048	-0.00235

Table 4: Location of c.g. and rotor hubs on joined-wing tilt-rotor aircraft.

	Body axis system coordinates		
	x (inches)	y (inches)	z (inches)
Component location:			
center of gravity	0.	0.	0.
right hub	49.40	192.99	-26.44
left hub	49.40	-192.99	-26.44

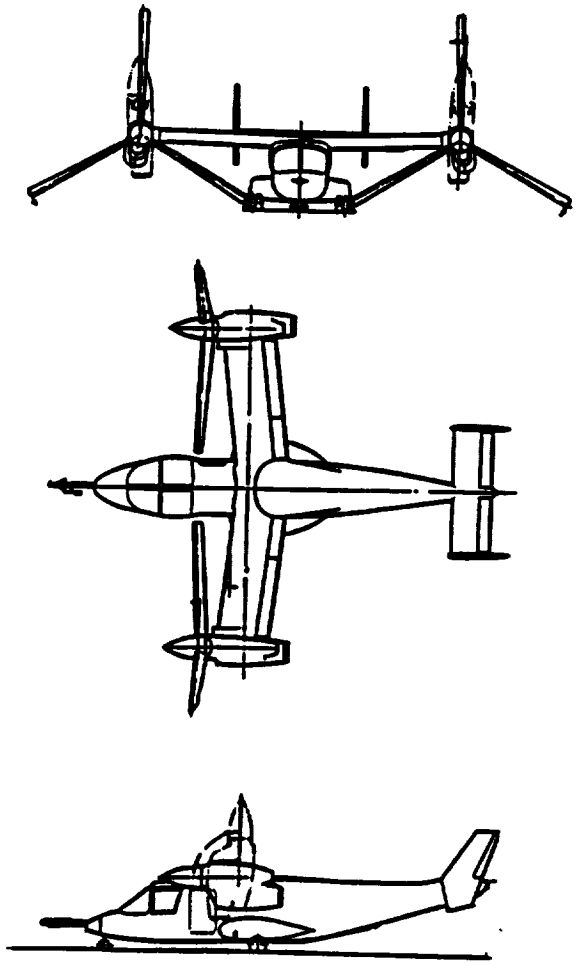

Fig. 1: Baseline cantilever-wing tilt-rotor configuration.

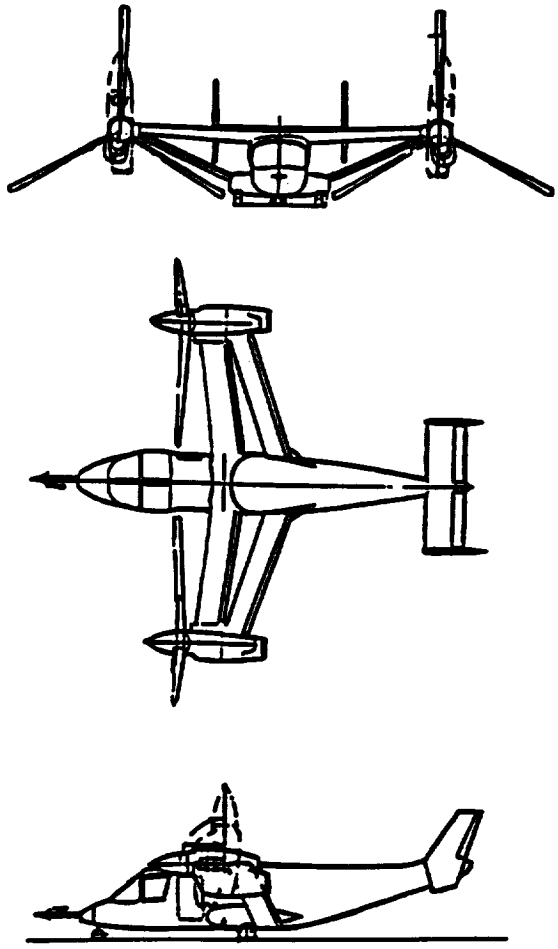

Fig. 2: Typical joined-wing tilt-rotor configuration.

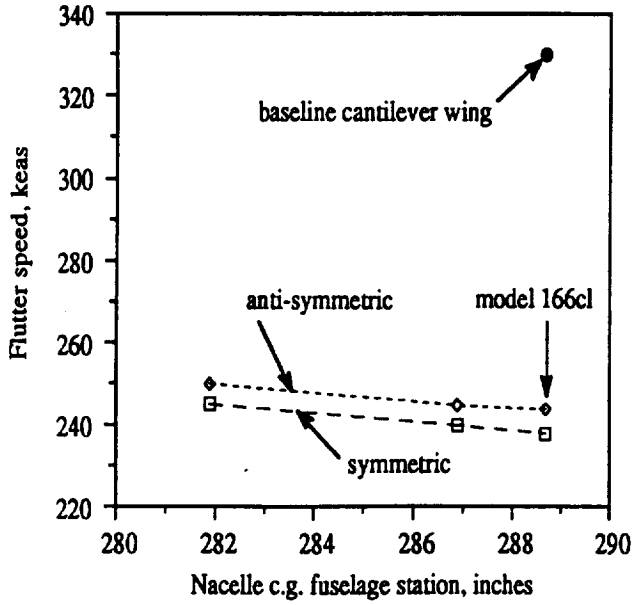

Fig. 3: Effect of nacelle c.g. location on the flutter speed of the joined-wing tilt-rotor aircraft (baseline cantilever-wing aircraft flutter speed shown for comparison). (source: Ref. 2)

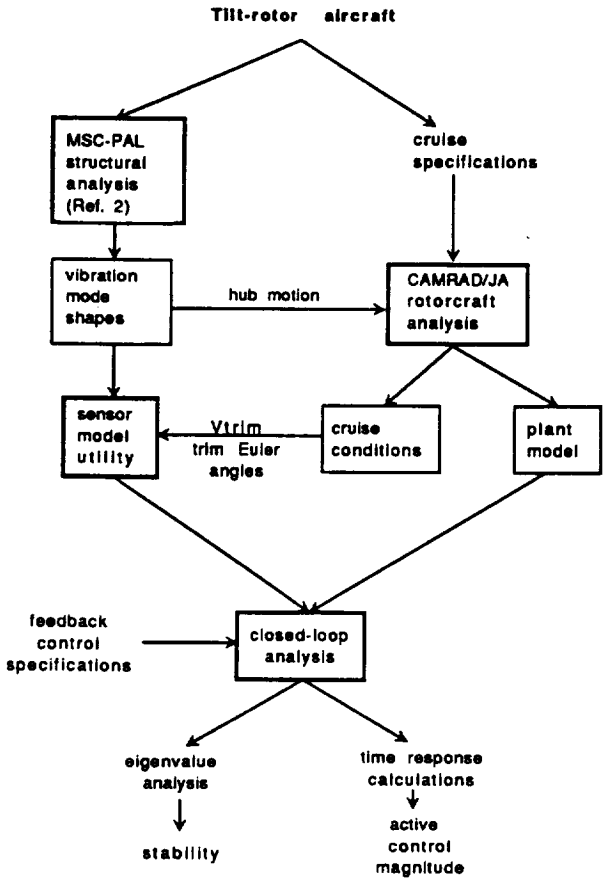

Fig. 4: Methodology of whirl-flutter alleviation study

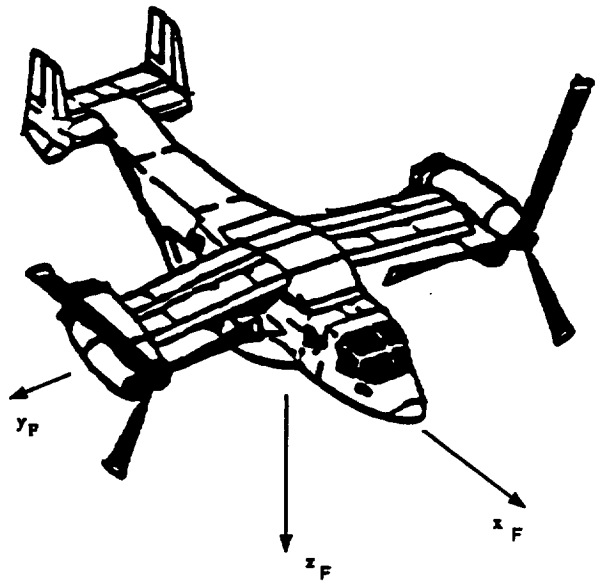

Fig. 5: Body axis system

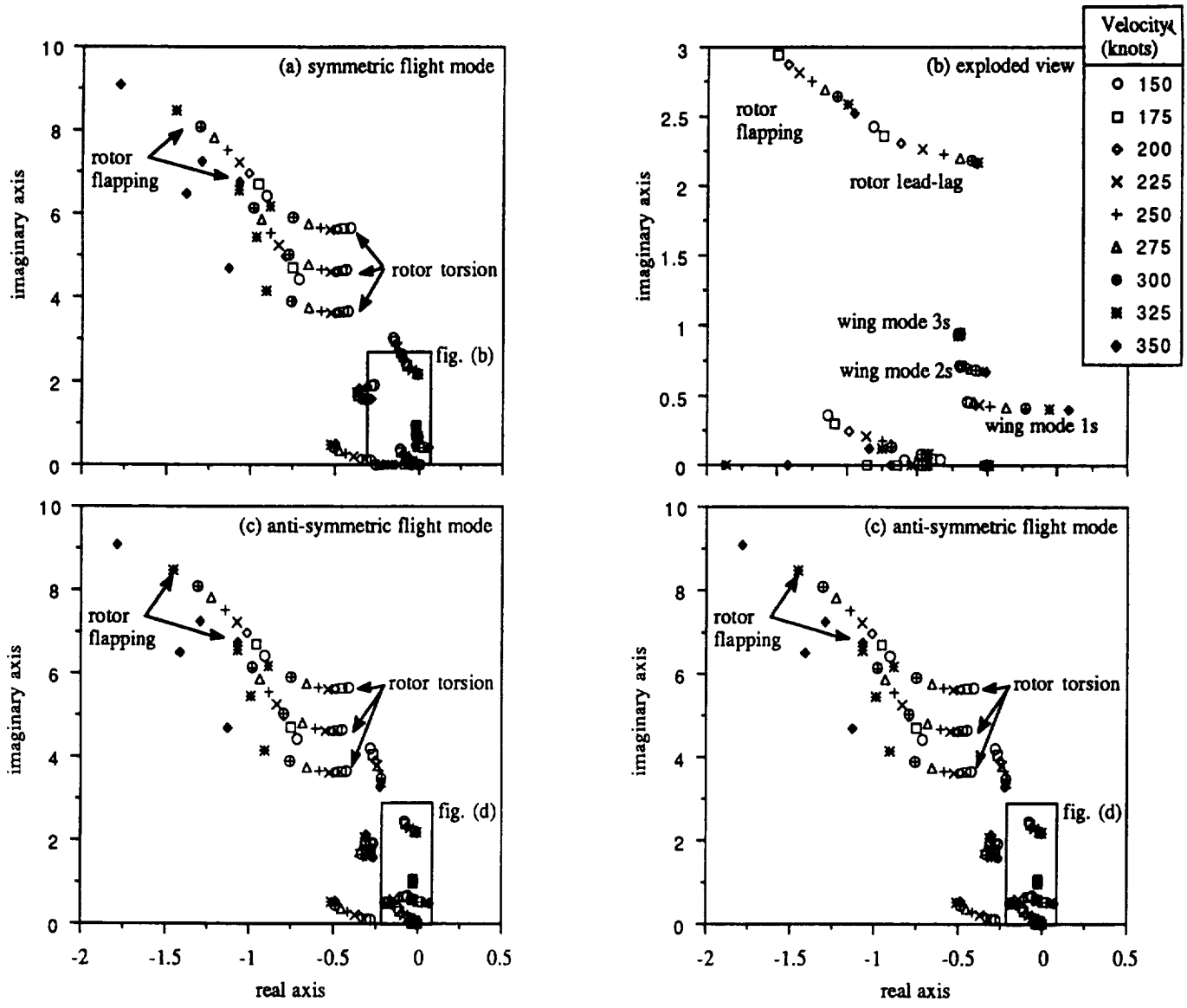

Fig. 6: Root locus plots for basic joined-wing aircraft without active controls.

(a) symmetric flight mode
(b) symmetric flight mode exploded view
(c) anti-symmetric mode
(d) anti-symmetric mode exploded view

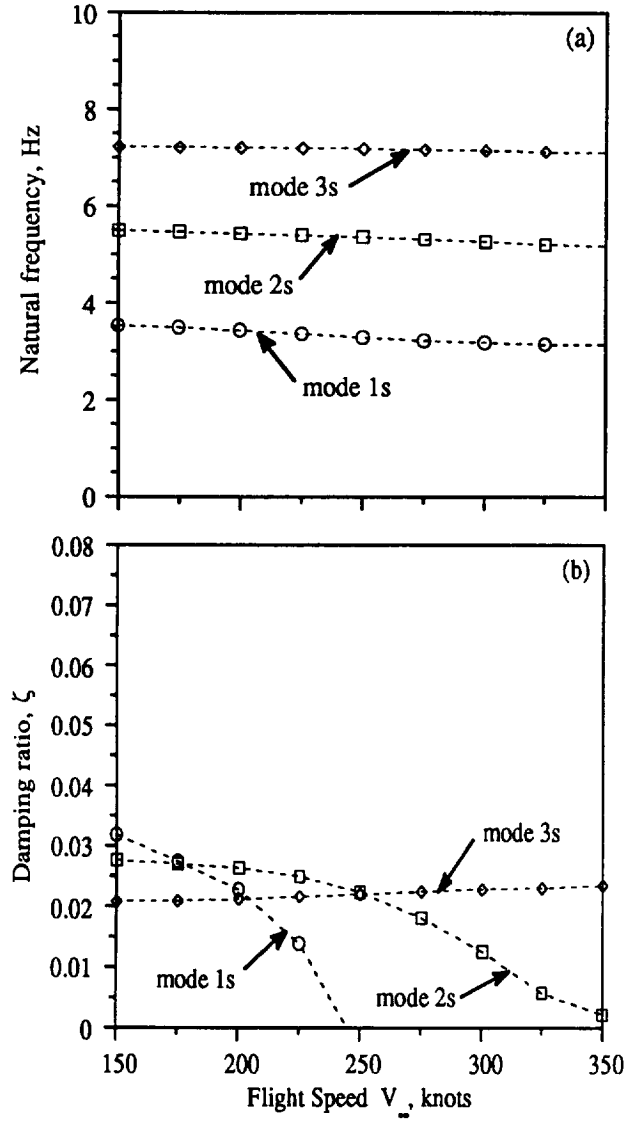

Fig. 7: Natural frequency and damping ratio of wing modes for basic aircraft without active controls, symmetric flight condition;
(a) Natural frequency, Hz
(b) Damping ratio, ζ

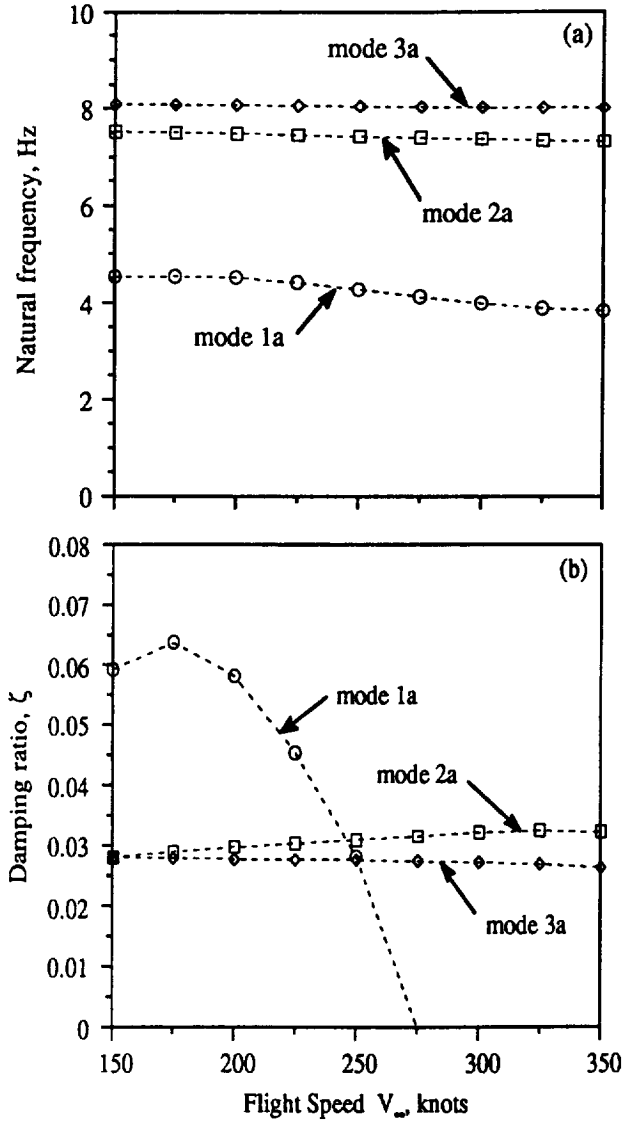

Fig. 8: Natural frequency and damping ratio of wing modes for basic aircraft without active controls, anti-symmetric flight condition;
(a) Natural frequency, Hz
(b) Damping ratio, ζ

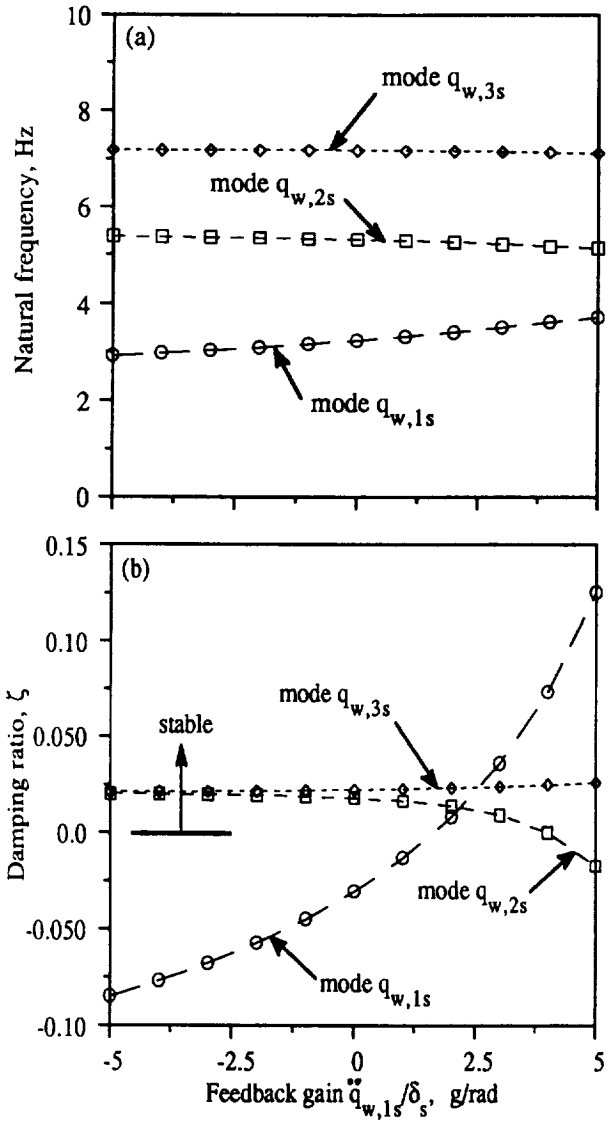

Fig. 9: Natural frequency and damping ratio for wing modes for closed loop system (symmetric flight mode) when feeding back wing mode state variable acceleration, $\ddot{q}_{w,1s}$, to longitudinal cyclic pitch, δ_s, at 275 knots

(a) Natural frequency, Hz
(b) Damping ratio, ζ

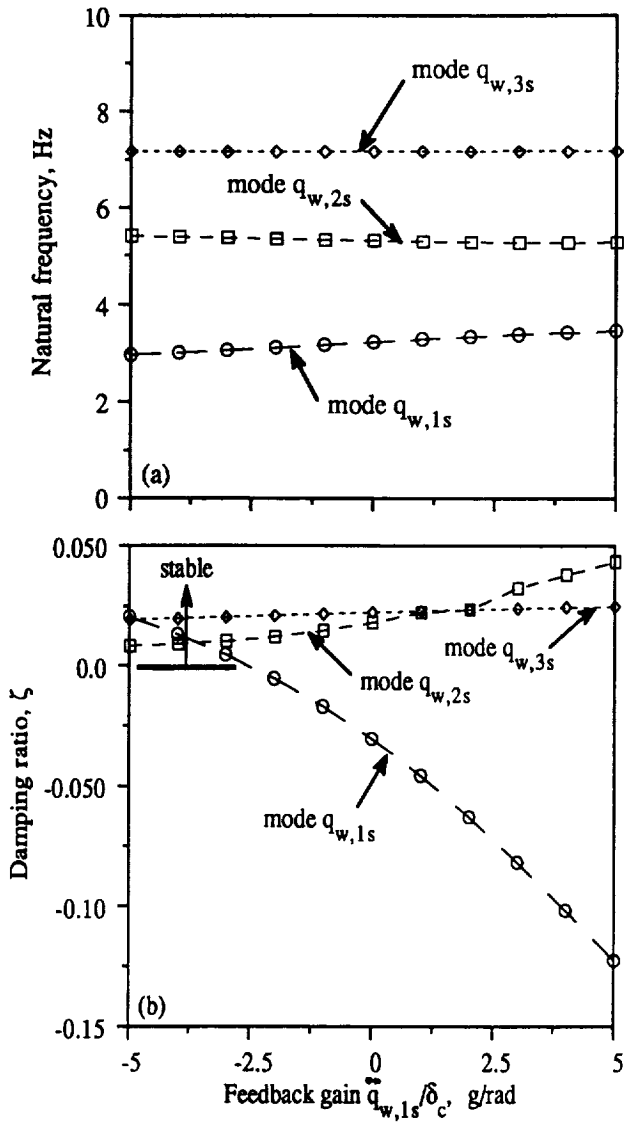

Fig. 10: Natural frequency and damping ratio for wing modes for closed loop system (symmetric flight mode) when feeding back wing mode state variable acceleration, $\ddot{q}_{w,1s}$, to lateral cyclic pitch, δ_c, at 275 knots

(a) Natural frequency, Hz
(b) Damping ratio, ζ

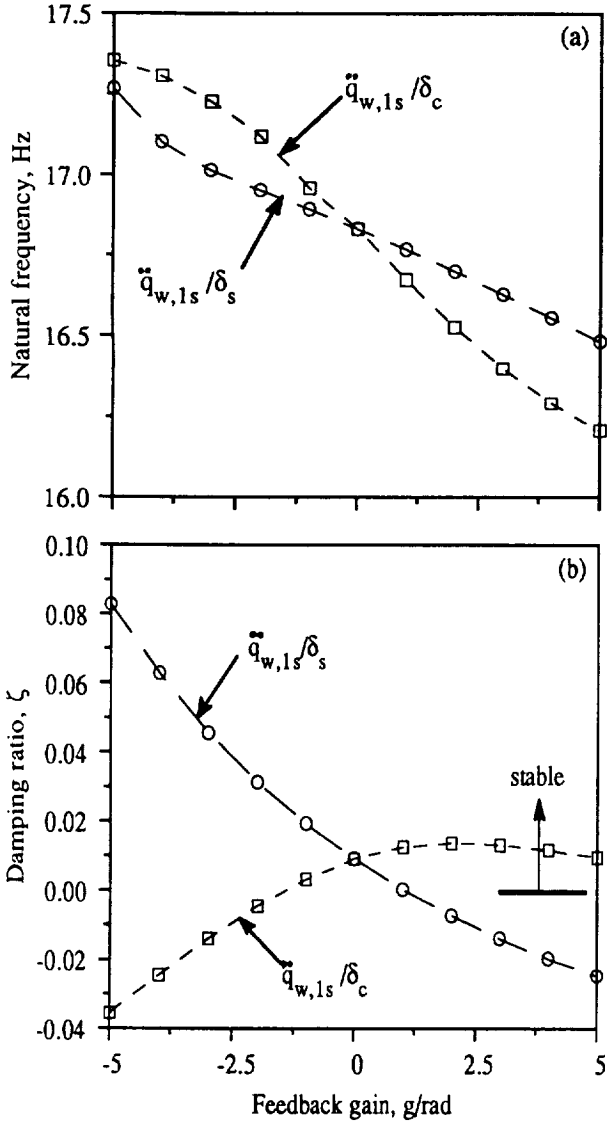

Fig. 11: Natural frequency and damping ratio for critical rotor mode for closed loop system (symmetric flight mode) when feeding back wing mode, $\ddot{q}_{w,1s}$ acceleration to longitudinal (δ_s) or lateral (δ_c) cyclic pitch at 275 knots.

(a) Natural frequency, Hz
(b) Damping ratio, ζ

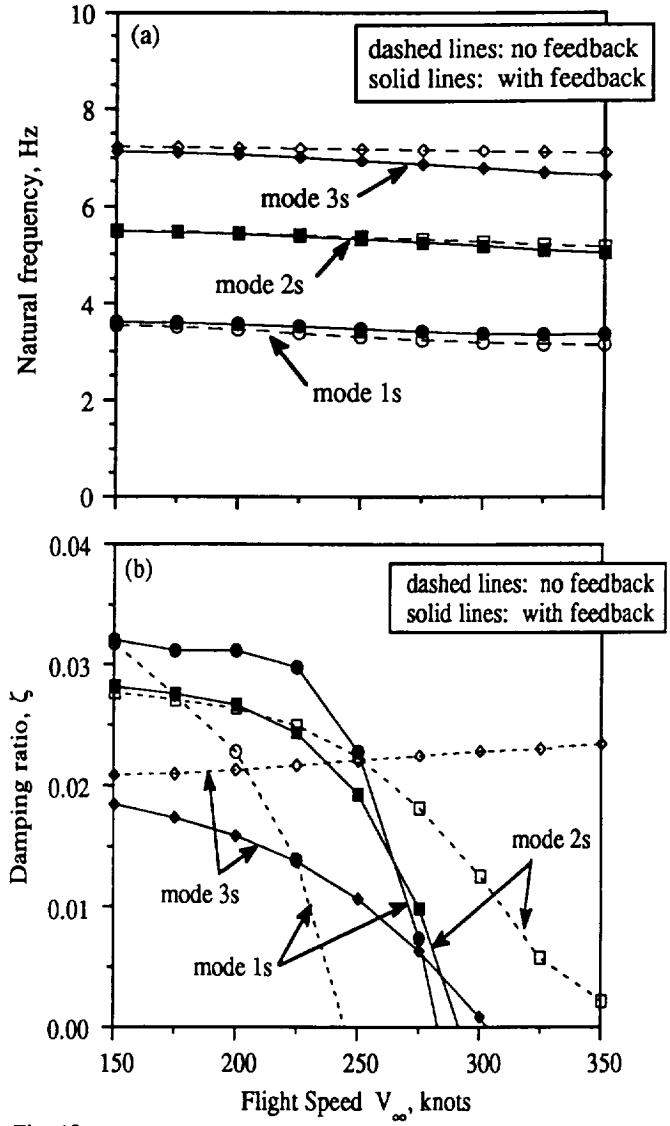

Fig. 12: Natural frequency and damping ratio for wing modes for basic aircraft and for closed loop system using sensors measuring state variable accelerations (symmetric flight mode): $\ddot{q}_{w,1s}/\delta_s$ = 2.0 g/rad, $\ddot{q}_{w,3s}/\delta_s$ = -1.25 g/rad

(a) Natural frequency, Hz
(b) Damping ratio, ζ

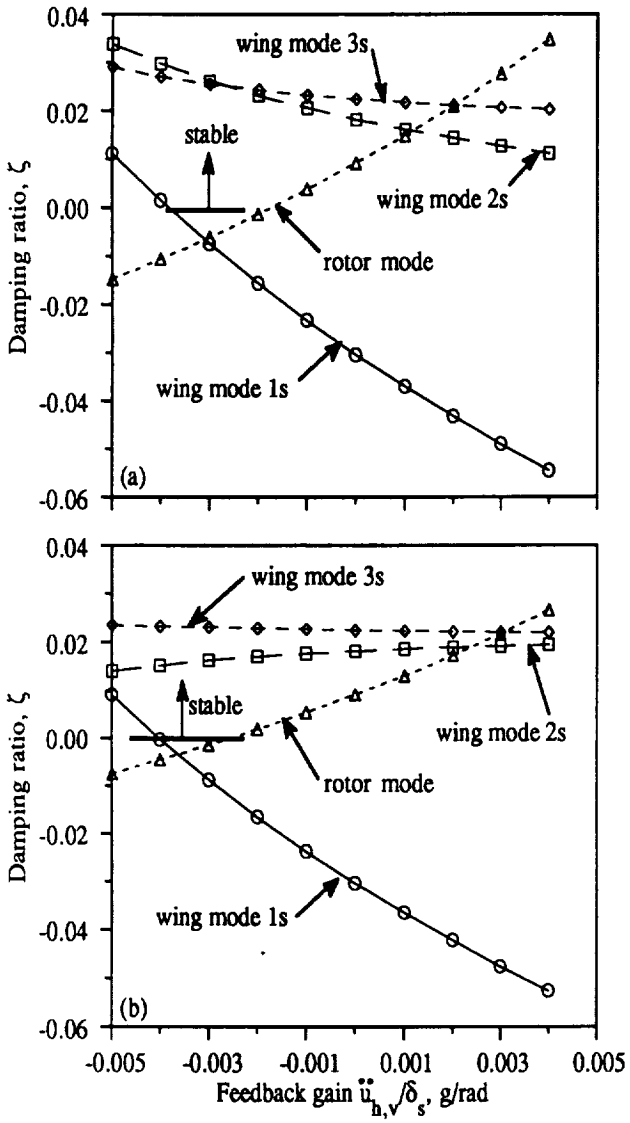

Fig. 13: Damping ratio for wing and critical rotor modes for closed loop system (symmetric flight mode) when feeding back vertical hub acceleration $\ddot{u}_{h,v}$ to longitudinal cyclic pitch.

(a) without a notch filter on vertical accelerometer output
(b) with a notch filter on vertical accelerometer output

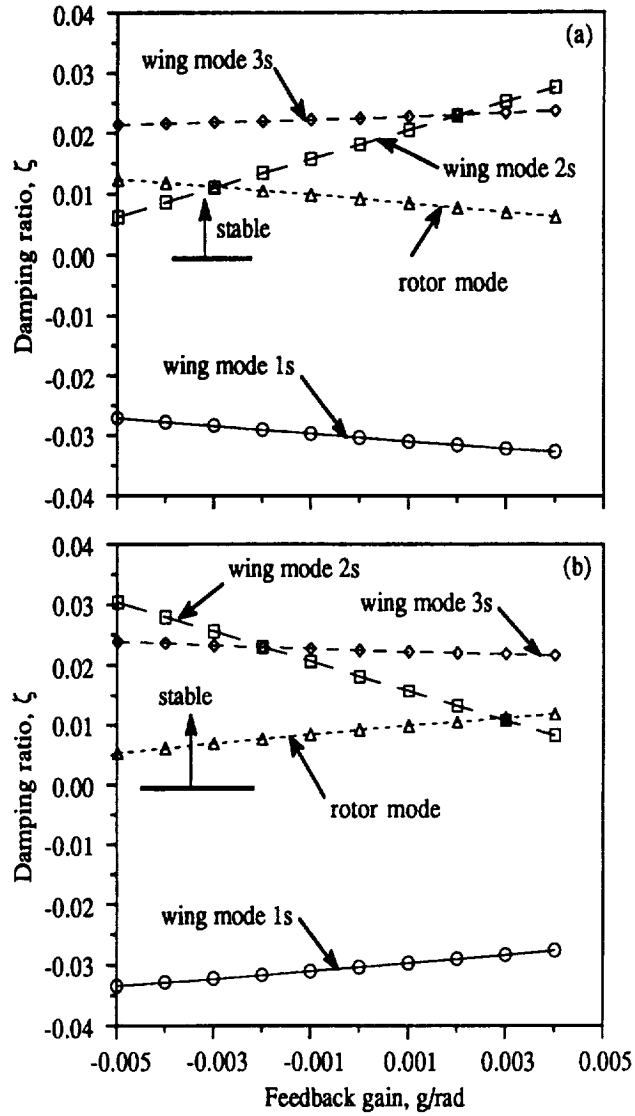

Fig. 14: Damping ratio for wing and critical rotor modes for closed loop system (symmetric flight mode) with feedback to longitudinal cyclic pitch.

(a) feeding back chord-wise hub acceleration, $\ddot{u}_{h,c}$
(b) feeding back span-wise hub acceleration, $\ddot{u}_{h,s}$

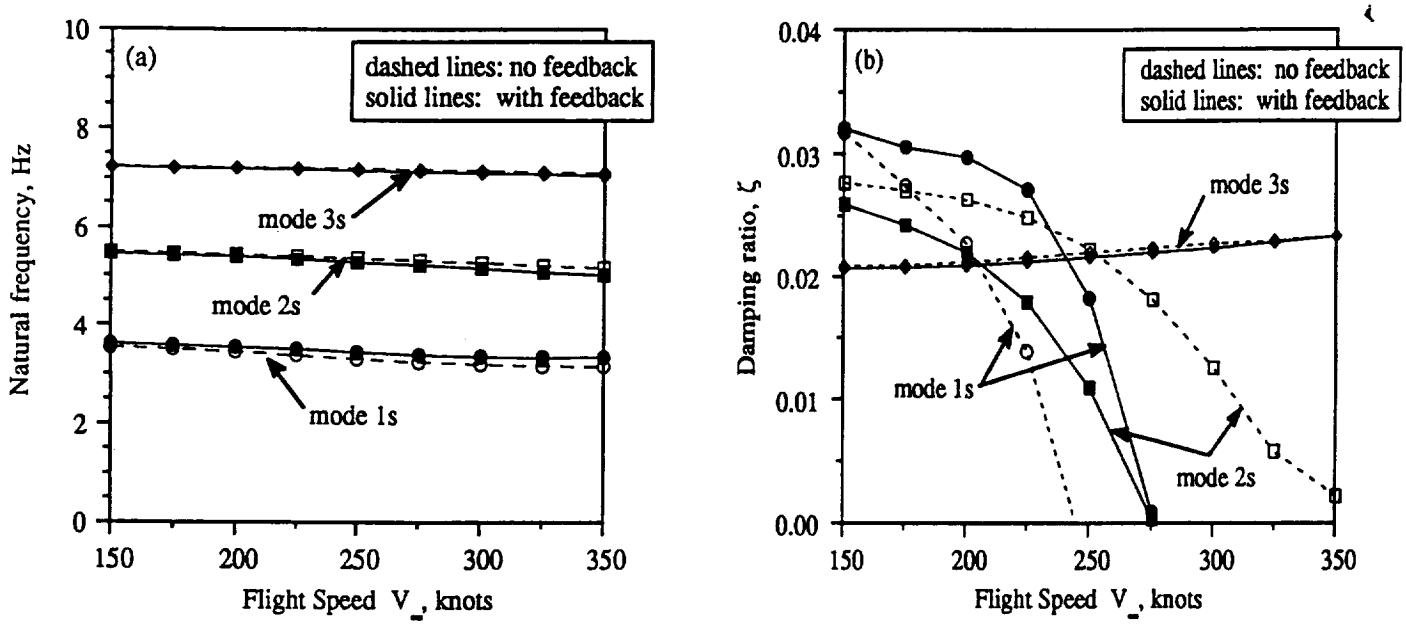

Fig. 15: Natural frequency and damping ratio for wing modes for basic aircraft and for closed loop system using sensor at hub measuring "physical" accelerations: $\ddot{u}_{h,s}/\delta_{s}$ = 0.0048 g/rad, $\ddot{u}_{h,v}/\delta_{s}$ = -0.0035 g/rad

(a) Natural frequency, Hz
(b) Damping ratio, ζ

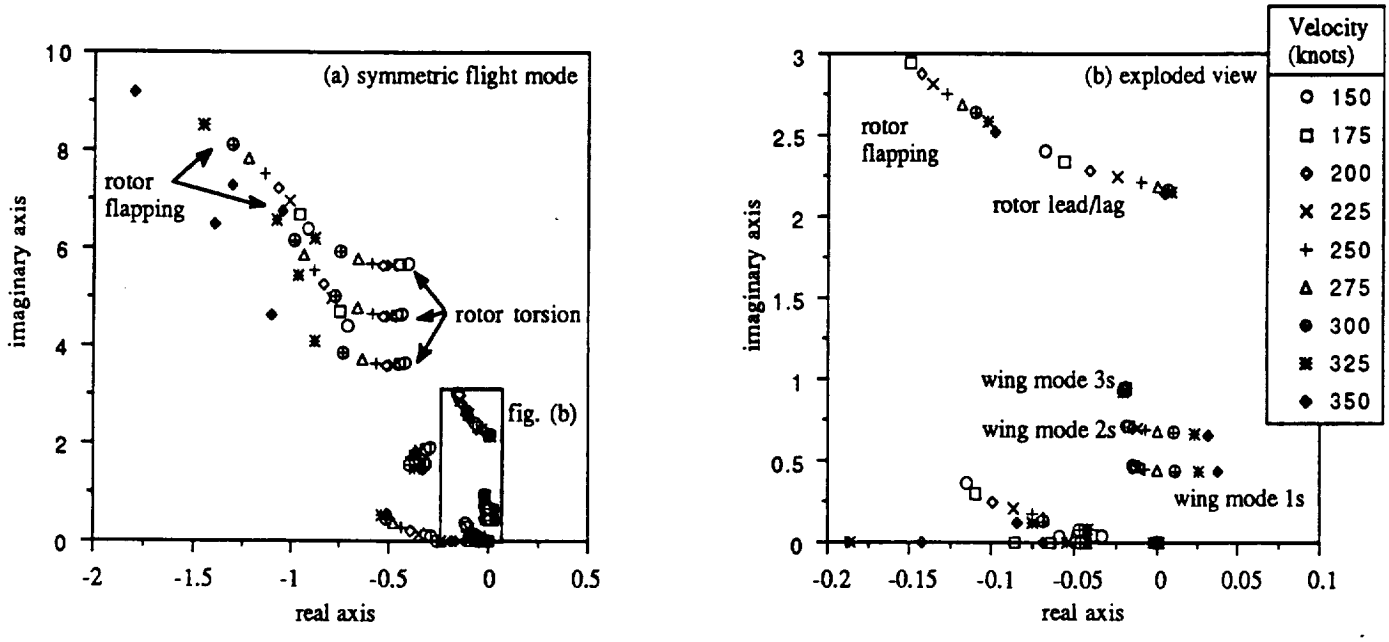

Fig. 16: Root locus plots for closed-loop system using feedback of vertical and spanwise accelerations at the hub to longitudinal cyclic pitch.

(a) symmetric mode
(b) symmetric mode exploded view

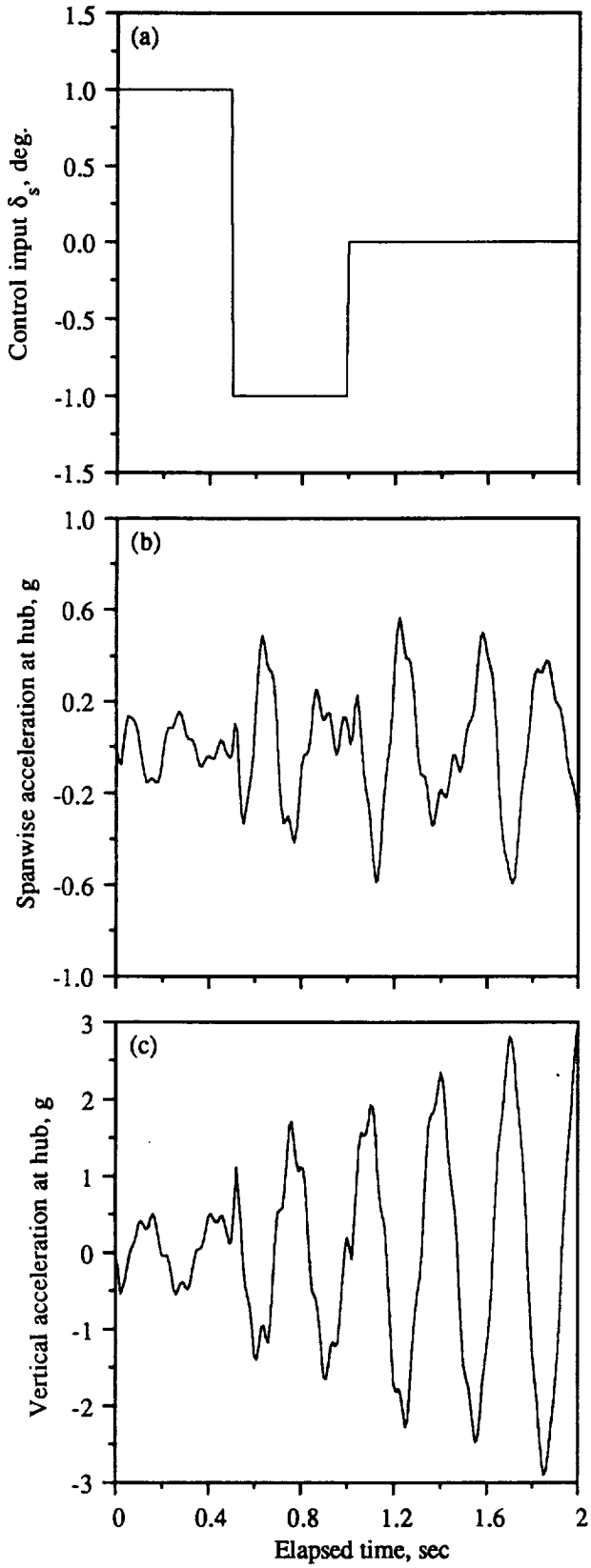

Fig. 17: Basic aircraft time response to a square doublet δ_s longitudinal cyclic pitch input;

(a) Active control input δ_s, deg

(b) Span-wise acceleration $\ddot{u}_{h,s}$, g

(c) Vertical acceleration $\ddot{u}_{h,v}$, g

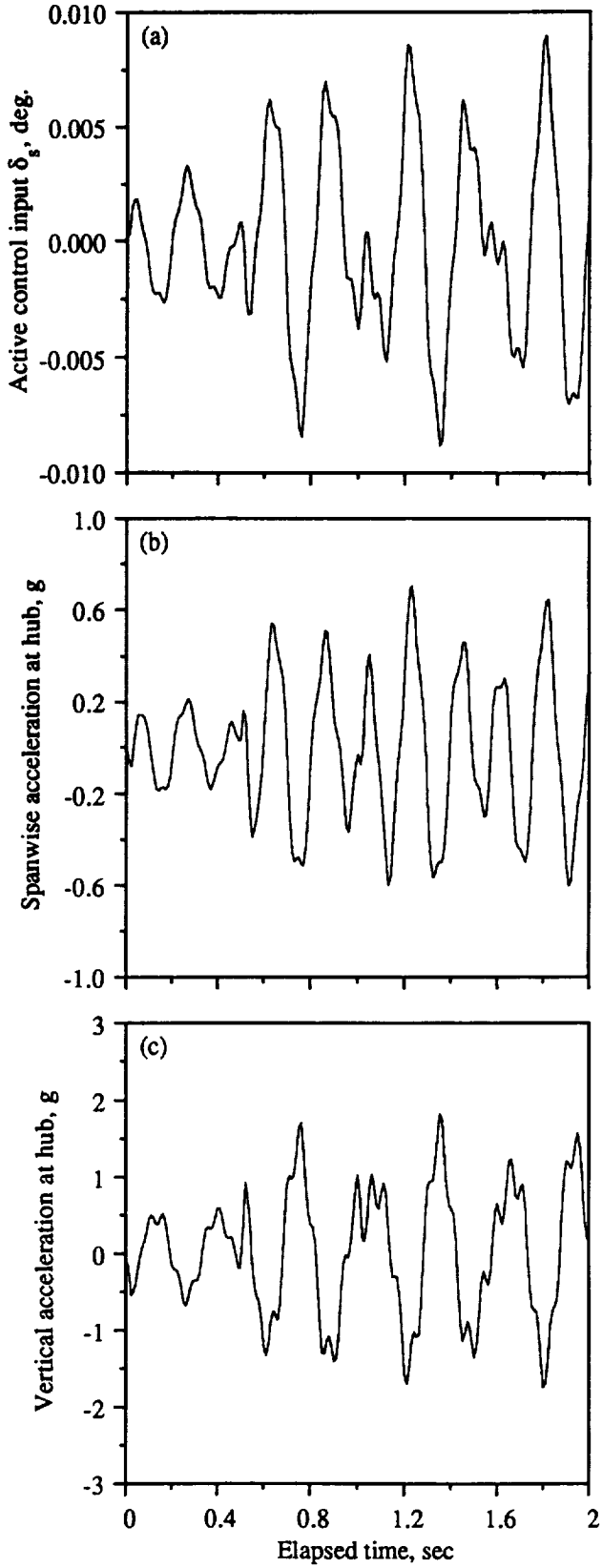

Fig. 18: Closed-loop time response to a square doublet δ_s input;

(a) Active control input δ_s, deg

(b) Span-wise acceleration $\ddot{u}_{h,s}$, g

(c) Vertical acceleration $\ddot{u}_{h,v}$, g

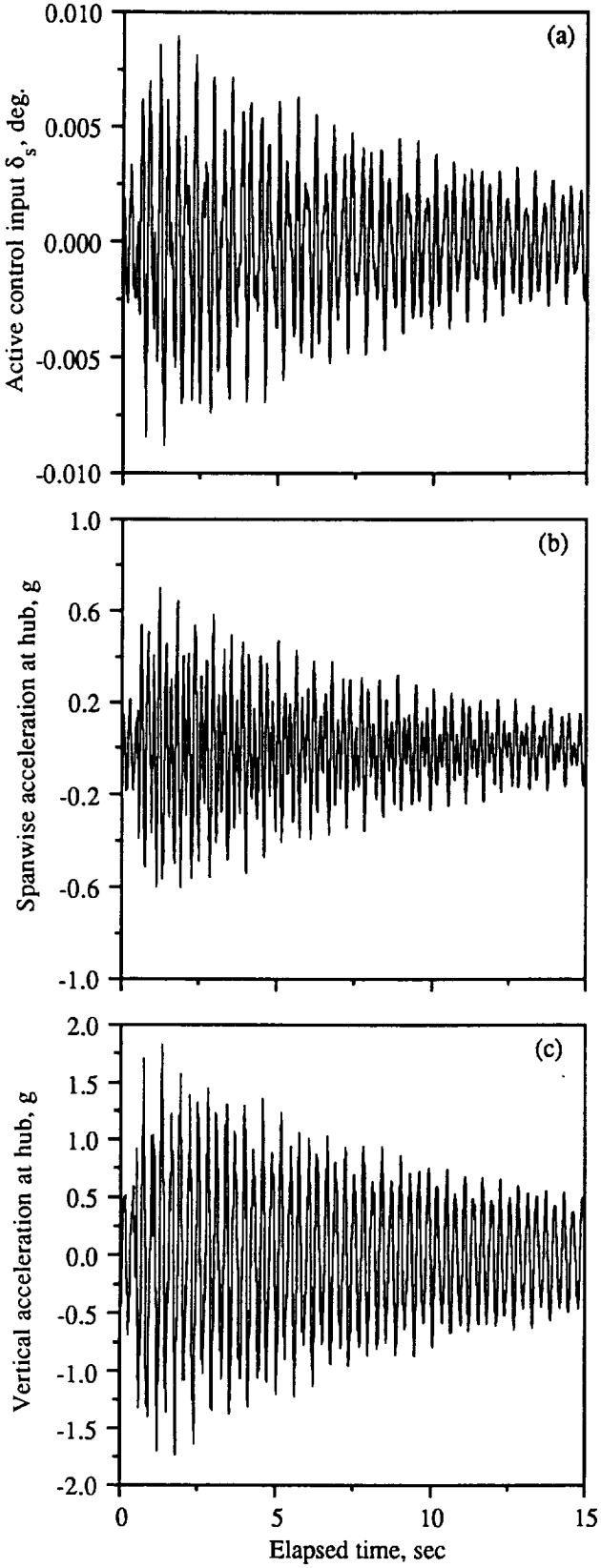

Fig. 19: Closed-loop time response to a square doublet δ_s input.

(a) Active control input δ_s, deg

(b) Span-wise acceleration $\ddot{u}_{h,s}$, g

(c) Vertical acceleration $\ddot{u}_{h,v}$, g

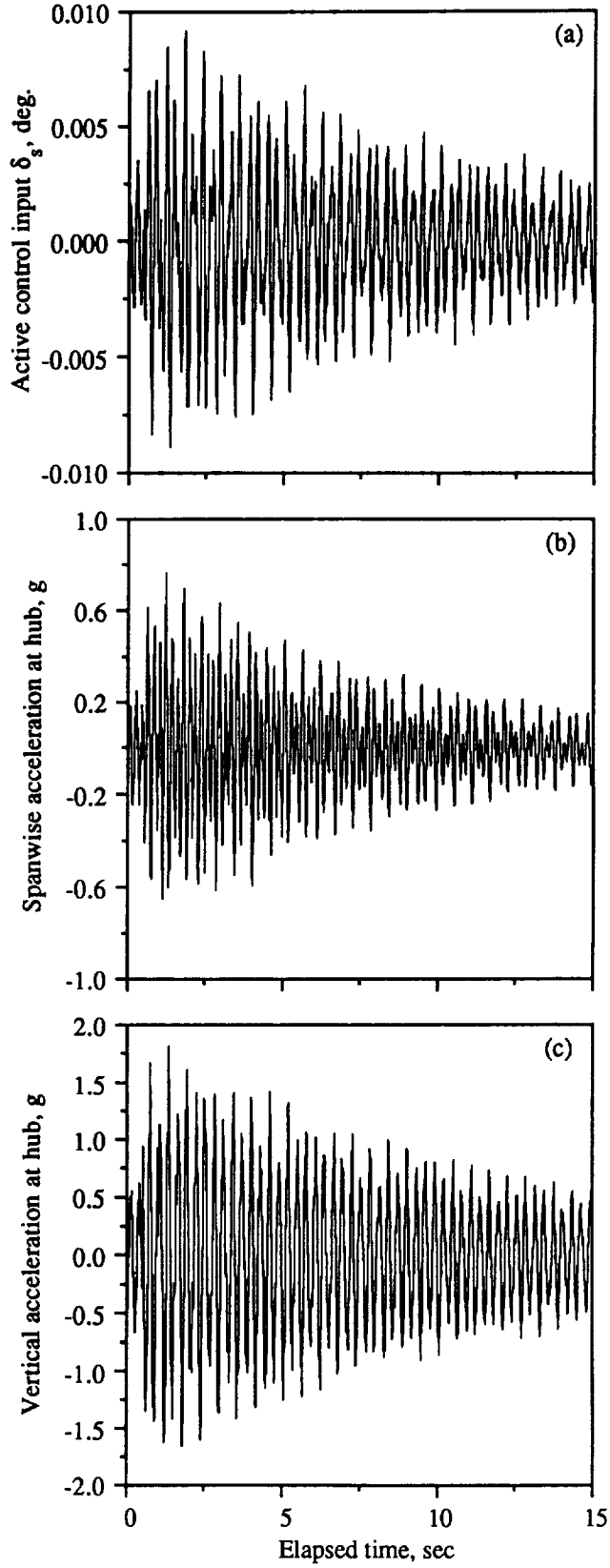

Fig. 20: Closed-loop time response to a square doublet δ_s input with a 0.1g sensor noise contamination.

(a) Active control input δ_s, deg

(b) Span-wise acceleration $\ddot{u}_{h,s}$, g

(c) Vertical acceleration $\ddot{u}_{h,v}$, g

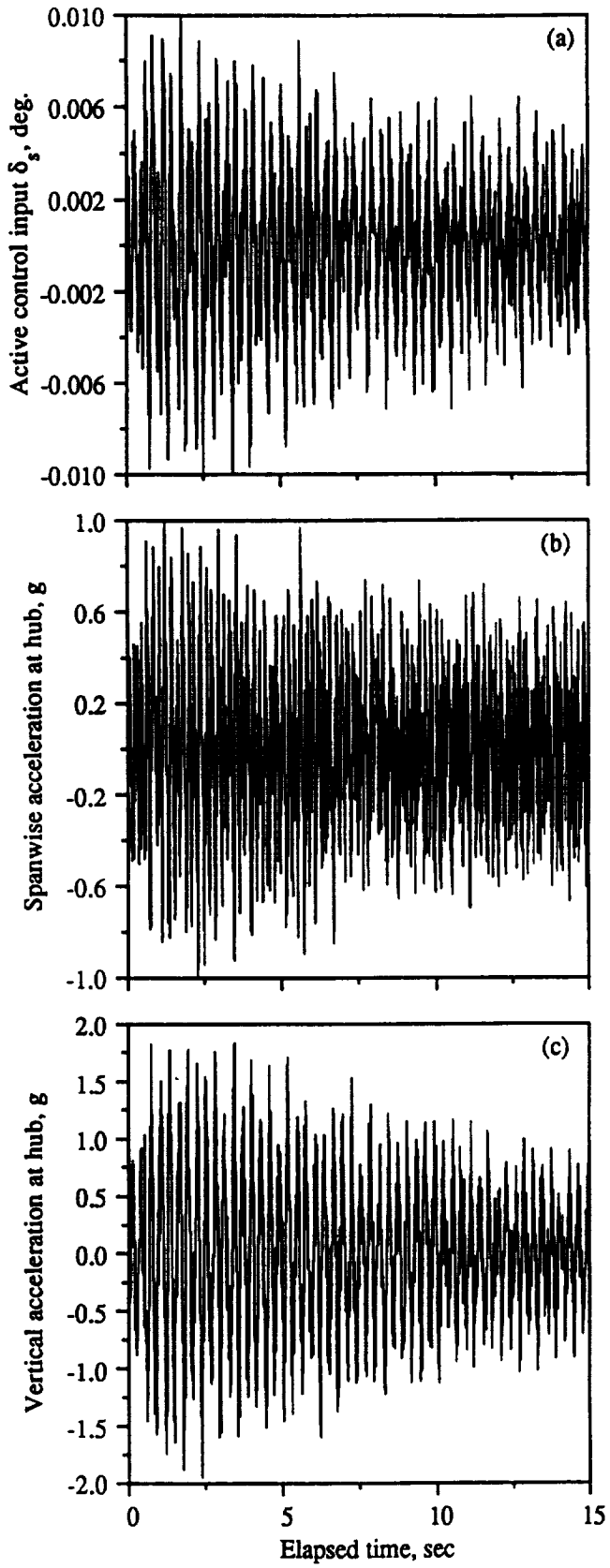

Fig. 21: Closed-loop time response to a square doublet δ_s input with a 0.5g sensor noise contamination.

(a) Active control input δ_s, deg

(b) Span-wise acceleration $\ddot{u}_{h,s}$, g

(c) Vertical acceleration $\ddot{u}_{h,v}$, g